

The author's responses to the reviewer's comments are merged below, and the revised manuscript is attached.

Response to Reviewer #1

We appreciate your time for carefully reviewing our manuscript. We would like to thank you for the constructive comments and suggestions, which encourage and help us to improve the manuscript. The manuscript has been revised accordingly. In the response below, your comments are provided in black text and [our responses are provided in blue text](#).

Response:

Using a total of 20 non-precipitating single-layer marine boundary layer (MBL) stratus and stratocumulus cloud cases over the eastern north Atlantic (ENA) ocean, this study investigates the impacts of the environmental variables on the aerosol-cloud interaction (ACIr). Interesting results have been found with valuable discussions. For example, it shows that the ACIr values vary from -0.004 to 0.207 with increasing precipitable water vapor (PWV) conditions, indicating that re is more sensitive to the CCN loading under sufficient water vapor supply, owing to the combined effect of enhanced condensational growth and coalescence processes associated with higher cloud droplets and PWV. The paper is also well written. I would recommend its acceptance for publication after necessary minor revisions.

Detailed comments;

Line 41-44, two “verbs” exist for this sentence, which should be rephrased. Also, a few more studies are recommended here, particularly the longwave radiative property change of clouds by aerosols, such as Garrett and Zhao (2006, Doi:10.1038/nature04636).

[The sentence is rephrased, and the citation is added.](#)

Line 48-52, a few similar studies have also been carried out over the western pacific regions, which might be worthy to mention, such as Zhao et al. (2019, Doi:10.3390/atmos10010019), and Yang et al. (2019, Doi:10.1016/j.atmosres.2019.01.027).

[The citations are added.](#)

Line 66-69, Qiu et al. (2017, Doi:10.1016/j.atmosenv.2017.06.002) showed negative relationship between cloud re and aerosol amount for low precipitable water vapor condition in spring, fall and winter at southern great plain site, but positive relationship between cloud re and aerosol amount for high precipitable water vapor condition, which could be also cited here. Similar findings have also been found over other locations, such as western pacific region near Hebei province, China.

[The citation is added.](#)

Line 281-283, similar height normalization method has been proposed and used by Zhao et al. (2018, Doi:10.1002/2017EA000346), which is worthy to mention here. Also, Similar findings (Line 283-287) have been found earlier in several studies, including the study mentioned here.

The citation is added, in section 3.5.1 of the revised manuscript.

Line 319, Eq. (2). Earlier studies often define this for fixed LWC. How could the different definition affect the results?

The LWC/LWP describes the liquid water (i.e., existing cloud droplets), so physically linked to the r_e and N_c . Mathematically, they have interdependent relationship in the cloud retrieval procedures, and hence to a certain extent, share the co-variabilities with the cloud microphysical properties (Dong et al., 1998; Wu et al., 2020a). In this study, by using the PWV as a sorting variable, we are trying to capture the role of ambient available water vapor in the cloud droplet growth process (especially the water vapor diffusional growth), using measurement independent to the cloud retrievals.

The discussion above is added, in section 3.3 of the revised manuscript.

Line 332-343, These are interesting findings and explanations. I wonder if this is related to the supersaturation adopted for CCN observed, or related to the true supersaturation status within clouds.

In order to investigate the theoretical implication of supersaturation conditions on the aerosol-cloud interaction observed here in the MBL stratiform clouds, the ACI_r values are calculated with respect to the surface N_{CCN} theoretically at two additional high supersaturation levels (0.5% and 1.2%), under all PWV_{BL} conditions. The results in Table 3 show that the ACI_r signals are both weak and do not have significant changes under relatively lower PWV_{BL} conditions, while the ACI_r signals tend to strengthen with the increase of supersaturation under the relatively higher PWV_{BL} . Based on the Köhler theory, if the supersaturation exceeds the critical point for the given droplet, the droplet will thus experience continued growth, so theoretically the ACI should increase with the supersaturation under same aerosol number concentration. However, the observed limited water vapor cannot support this ideal droplet growth, results in weak responses of cloud droplets to aerosol intrusion. With the increase of observed water vapor, the continued growth of cloud droplets becomes more plausible, hence the high supersaturation yields larger droplets with low number of aerosols, more efficient droplet activation with a large number of aerosols, and in turns, larger ACI_r (even out of the theoretical bounds). However, considering these high supersaturation environments are unphysical in the observed MBL cloud layers, and estimating the real supersaturation conditions using ground-based remote-sensing is beyond the scope of this study, we

67 chose the supersaturation level of 0.2% because it represents the most typical supersaturation conditions
 68 of MBL stratiform clouds.

Table 3. ACI_r calculated with respect to N_{CCN} theoretically at different supersaturation levels, under all PWV_{BL} conditions

PWV_{BL} (cm)	0.4-0.6	0.6-0.8	0.8-1.0	1.0-1.2	1.2-1.4	1.4-1.6	1.6-1.8	1.8-2.0	2.0-2.2	2.2-2.4
ACI_r ($N_{CCN}@0.2\%SS$)	0.020	0.057	0.002	-0.014	0.108	0.076	0.145	0.151	0.221	0.175
($N_{CCN}@0.5\%SS$)	0.023	0.057	0.0002	0.024	0.129	0.121	0.309	0.136	0.293	0.159
($N_{CCN}@1.2\%SS$)	0.023	0.045	0.002	0.072	0.125	0.123	0.323	0.175	0.347	0.186

69
 70 The discussion above is added, in the last paragraph of section 3.3 of the revised manuscript.

71
 72 Line 358-376, The mechanism proposed here is valuable. If possible, I would suggest the authors
 73 illustrate the mechanism proposed here with a diagram.

74 The diagram is added as Figure 8 in the revised manuscript as follows:

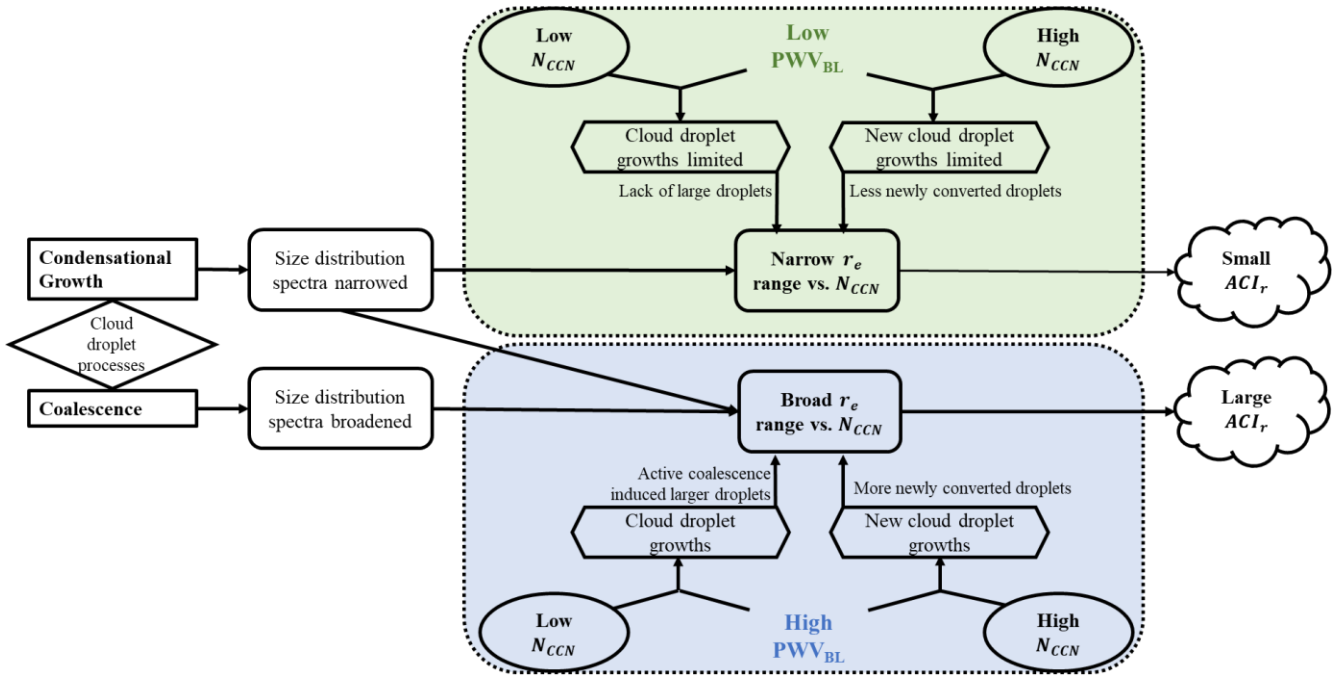


Figure 8. Theoretical mechanism of the responses of cloud droplet size distributions to different CCN intrusion, under relative insufficient (low PWV_{BL}) versus sufficient (high PWV_{BL}) water vapor availabilities.

75 Line 390, "that more close to adiabatic" should be "that are more close to adiabatic"

76 This sentence is removed in the revised manuscript.

77 Line 432, "to narrows the DSD" should be "to narrow the DSD"

78 The word 'narrows' is changed to 'narrow'.

Response to Reviewer #2

We appreciate your time for carefully reviewing our manuscript. We would like to thank you for the constructive comments and suggestions, which encourage and help us to improve the manuscript. The manuscript has been revised accordingly. In the response below, your comments are provided in black text and our responses are provided in blue text.

Response:

As the title suggests, this paper describes an aggregated analysis of aerosol-cloud interaction (ACI) in non-precipitating marine boundary layer clouds at the Eastern North Atlantic ARM remote sensing supersite. A relatively narrow view of ACI is taken in which the bivariate relationship between aerosol and cloud drop number concentration and the ACI index were calculated numerous times, compositing by various column-mean or column-integral quantities (e.g., water vapor path, cloud adiabaticity, lower tropospheric, turbulence). My main concern with the study is that each of these purported controlling factors is analyzed in isolation, which implicitly assumes no covariability among them. This assumption is not valid and no attempt to address this issue was given. As such, I find it difficult to accept many of the mechanistic arguments made by the authors. They cannot demonstrate cause and effect, and there are clearly confounding variables that limit their ability to draw stronger conclusions (for example, lines 243-244: “the coincidence of high NCCN and PWV does not necessarily imply a physical relationship”). I therefore recommend the manuscript be rejected and the authors encouraged to resubmit after broadening their analysis. The premise of evaluating ACI with the authors’ retrieval product is promising, but to understand the role of the controlling factors, they must be analyzed in a multi-dimensional framework (principal component analysis, k-means clustering, etc.) that allows the authors to identify and, more importantly, interpret co-variability among environmental factors. As it currently stands, the conclusions of this study point vaguely toward correlations with large-scale variables but give no clear guidance.

Thanks for the constructive suggestions. To better address the reviewer’s concern about the co-variabilities between the environmental variables and to more clearly shed light on their impacts on ACI, we have now conducted the principal component analysis (PCA). The variables of sub-cloud precipitable water vapor (PWV_{BL}), the boundary layer decoupling index (D_i), the vertical component of the turbulence kinetic energy (TKE_w), the lower tropospheric stability (LTS) and the surface wind directions in terms of northerly and southerly ($W_{dir,NS}$) are constructed as the input of the eigenanalysis. Results show that the first three PCs can describe the majority (~84%) of the variance among the selected variables. Where the most explanatory PC1 (account for 43.72% contribution) strongly correlated with

PWV_{BL}, D_i (both negatively) and TKE_w (positively), and hence describe the co-variation of the boundary layer conditions. While the PC2 and PC3 (account for 22.01% and 18.26% contributions, respectively) are strongly correlated with the LTS and $W_{dir,NS}$, which likely indicates the variations of the Azores High position and strength. By projecting the variables onto PC1 and PC2, the PCA loading analysis shows that the TKE_w are strongly negatively correlated with D_i , which as expected since a more decoupled MBL is often separated into two layers where the lower one can cap the surface moisture, while the higher TKE_w denote sufficient turbulence that maintains the well-mixed MBL. Additionally, the island effect is also indicated by the eigenanalysis, where the surface northerly wind would induce additional updraft velocity and hence disturb the TKE_w, owing to the topographic effect of the cliff north of the ENA site. Upon the PCA results, the role of cloud adiabaticities on the behaviors of CCN- N_c conversion is further examined using both binning and eigenanalysis. And the factors that have the most influence on the explanatory PCs are selected as the sorting variables in the ACI_r assessments.

The detailed discussions on the multi-dimensional PCA have been added to the section 3.4 of the revised manuscript as follows:

3.4 The co-variabilities of the meteorological factors

The environmental conditions over the ENA have been widely studied as not independent but entangled with each other (Wood et al., 2015; Zheng et al., 2016; Wu et al., 2017; Wang et al., 2021). To better understand the dependencies and the co-variabilities of the meteorological factors, a principal component analysis (PCA) is performed targeting on the following variables: (1) PWV_{BL} denotes the water vapor availabilities within the boundary layer; (2) D_i describes the boundary layer coupling conditions; (3) TKE_w represents the strength of boundary layer turbulence; (4) $W_{dir,NS}$ reflects the surface wind directions in terms of northerly and southerly; and (5) LTS infers the large-scale thermodynamic structures. Note that the $W_{dir,NS}$ are taken as $W_{dir,NS} = \text{abs}(W_{dir} - 180^\circ)$, so that the original W_{dir} (0-360°) can be transformed to $W_{dir,NS}$ (0-180°) where the values smaller than 90° are close to the southerly wind, and those greater than 90° are close to the northerly wind. The $W_{dir,ns}$ are transformed as such to capture the island effects better, because the cliff is located north of the ENA site.

The input data metric is constructed from the above five variables to apply the PCA, and the principal components (PCs) that serving to explain the variation of those dependent variables can be output from the eigenanalysis. The result shows that for the five selected meteorological factors, the proportions of the total intervariable variance explained by the PCs are 43.72%, 22.01%, 18.26%, 8.95% and 7.06%, and the eigenvalues are 2.19, 1.10, 0.91, 0.45, and 0.35, respectively. Note that the first three

146 PCs have the highest eigenvalues and explain most (~84%) of the total variance, which indicates that
 147 they can capture the significant variation patterns of the selective meteorological factors.

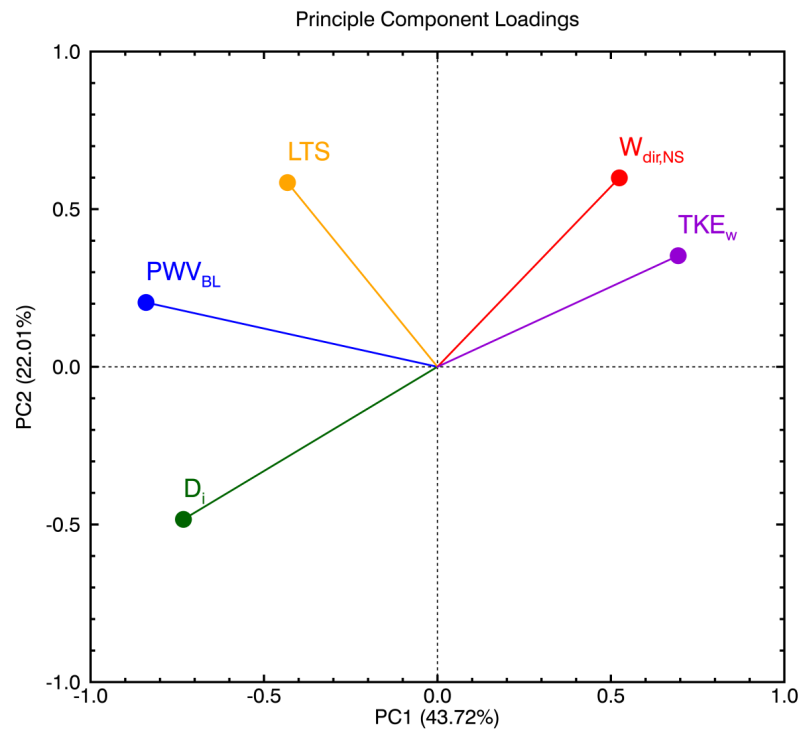
148 To determine the relative contributions of the variables to PCs, all the five selected meteorological
 149 variables are projected to the first three PCs and the Pearson correlation coefficients between them are
 150 listed in Table 4. For the first PC (PC1) which accounts for the highest proportion (43.72%) of the total
 151 variance, the PC1 is strongly negatively correlated with PWV_{BL} (-0.84) and D_i (-0.73), but strongly
 152 positively correlated with TKE_w (0.69). These results suggest that PC1 mainly represents the boundary
 153 layer conditions, and the co-variations of the boundary layer water vapor and turbulence are the most
 154 distinct environmental patterns for the selected cloud cases. The PC2 and PC3 are most correlated with
 155 LTS (0.58 and 0.65 for PC2 and PC3, respectively) and $W_{dir,NS}$ (0.60 and -0.50 for PC2 and PC3,
 156 respectively), indicating that the PC2 and PC3 mainly describe the variations in large-scale
 157 thermodynamic and the surface wind patterns, which are likely associated with the variations of the
 158 Azores High position and strength (Wood et al., 2015).

Table 4. The first three principal components from eigenanalysis

Eigenanalysis	PC1	PC2	PC3
Eigenvalues	2.17	1.10	0.91
Proportion of variance explained (%)	43.72	22.01	18.26
Cumulative proportion (%)	43.72	65.73	83.99
Correlations (Variables vs. PCs)	PC1	PC2	PC3
PWV_{BL}	-0.84	0.20	-0.11
D_i	-0.73	-0.48	-0.20
TKE_w	0.69	0.35	-0.44
$W_{dir,ns}$	0.52	0.60	-0.50
LTS	-0.43	0.58	0.65

159 To further understand the correlations between the meteorological variables, the principal
 160 component loadings plot is constructed by projecting the variables onto PC1 and PC2 as shown in Fig.
 161 4. Each point denotes the variable correlations with PC1 (x-coordinate) and PC2 (y-coordinate), so that
 162 each vector represents the strength and direction of the original variable influences on the pair of PCs.
 163 The angle between the two vectors represents the correlation between each other. In Fig. 4, both TKE_w
 164 and $W_{dir,NS}$ vectors are located in the same quadrant (positive in both PC1 and PC2) and close to each
 165 other with a small degree of an acute angle, which means the TKE_w are strongly correlated with the
 166 $W_{dir,NS}$. When the surface wind is coming from the north side of the island, the topographic lifting effect
 167 of the cliff would induce additional updraft over the ENA site (Zheng et al., 2016), so that the wind closer
 168

169 to the northerly wind (larger $W_{dir,NS}$) is more correlated with higher TKE_w . Note that TKE_w and D_i
 170 vectors are almost in an opposite direction, which denotes a strongly negative correlation between the
 171 two variables. The angles of PWV_{BL} with D_i ($\sim 45^\circ$) and TKE_w ($\sim 142^\circ$) suggest that PWV_{BL} is
 172 moderately positively correlated with D_i but negatively correlated with TKE_w . A higher D_i indicates a
 173 more decoupled MBL, where MBL is not well-mixed and separated into a radiative-driven layer and a
 174 surface flux driven layer that caps the surface moisture (Jones et al., 2011). This situation is more likely
 175 to associate with a relatively higher PWV_{BL} and weaker TKE_w condition. As for the LTS parameter, the
 176 close to 90° angle with TKE_w suggests no correlation between them, since the LTS is mostly capturing
 177 the large-scale thermodynamical structures and is obtained from a coarser temporal resolution. Thus, the
 178 LTS does not essentially have correspondence to the strength of boundary layer turbulence and can be
 179 treated as independent to TKE_w over the ENA site. The loading plot intuitively tells us the directions and
 180 strengths of the co-variabilities of the selected meteorological variables, and sheds the light on
 181 determining the key factors that are feasible to use in examining the environmental impacts on the
 182 aerosol-cloud interactions.



183 **Figure 4.** The projections of TKE_w (purple), $W_{dir,NS}$ (red), LTS (orange), PWV_{BL} (blue) and D_i (green)
 onto the first principal component (PC1) and the second principal component (PC2). The x-coordinates
 denote variables' correlations with PC1, and the y-coordinates denote variables' correlations with PC2.

184

185 In addition, the detailed results and discussions on the impacts of meteorological factors on
186 aerosol and cloud properties, and aerosol-cloud interactions can be found in the section 3.5 of the revised
187 manuscript.

188
189
190 I have a number of other concerns the authors may also wish to consider:

- 191 •How good of a proxy is PWV for PBL relative humidity? Are there cases when non-drizzling
192 stratocumulus occur with a relatively moister free troposphere? Perhaps you could estimate the
193 fraction of PWV in the PBL using the interpolated sonde product or Raman lidar (note: Raman
194 will only get you subcloud vapor)?

195 Thanks for the comment and suggestions. In the revise manuscript, we changed to use the sub-cloud
196 boundary-layer PWV (PWV_{BL}), and tested the contribution of PWV_{BL} to column PWV. The discussion
197 has been added to the section 2.2 in the revised manuscript as follows:

198
199 To capture the information of MBL water vapor more accurately, the sub-cloud boundary layer
200 integrated precipitable water vapor (PWV_{BL}) is calculated using the interpolated sounding product
201 following:

$$202 \quad PWV_{BL} = \frac{1}{\rho_w} \sum (z_{i+1} - z_i) * (\rho_{v,i+1} + \rho_{v,i}) / 2, \quad (1)$$

203 where the ρ_w is the liquid water density and the ρ_v is the water vapor density collected from the
204 Interpolated Sounding and Gridded Sounding Value-Added Products (Toto and Jensen, 2016), the
205 subscripts i and $i + 1$ represent the bottom and top of each interpolated sounding height layer. Both
206 PWV and PWV_{BL} are temporally collocated to 5-min resolution and plotted against each other in Fig.
207 S1a to test the contribution of PWV_{BL} to the PWV. The Pearson correlation coefficient of 0.85 shows
208 that the PWV_{BL} are strongly positively correlated with the PWV, while the distribution of the percentage
209 ratio of PWV_{BL} to PWV (Fig. S1b) indicates that, on average, the PWV_{BL} contribute to ~58% of the
210 PWV. Considering the cloud-topped MBL, the majority of cases (~74%) associate with a relatively moist
211 boundary layer compared to the amount of water vapor in the free troposphere, where the PWV_{BL} already
212 contributed over 50% of the total column PWV. In contrast, only ~9% of cloud samples occur under a
213 relatively dry boundary layer and moist free troposphere, where PWV_{BL} contributions are less than 40%.
214 In general, the PWV can well capture the variation of the PWV_{BL} . In the rest of the study, the PWV_{BL}

215 are used, as it represents the sub-cloud boundary layer water vapor availabilities which are more closely
 216 related to the MBL cloud processes.

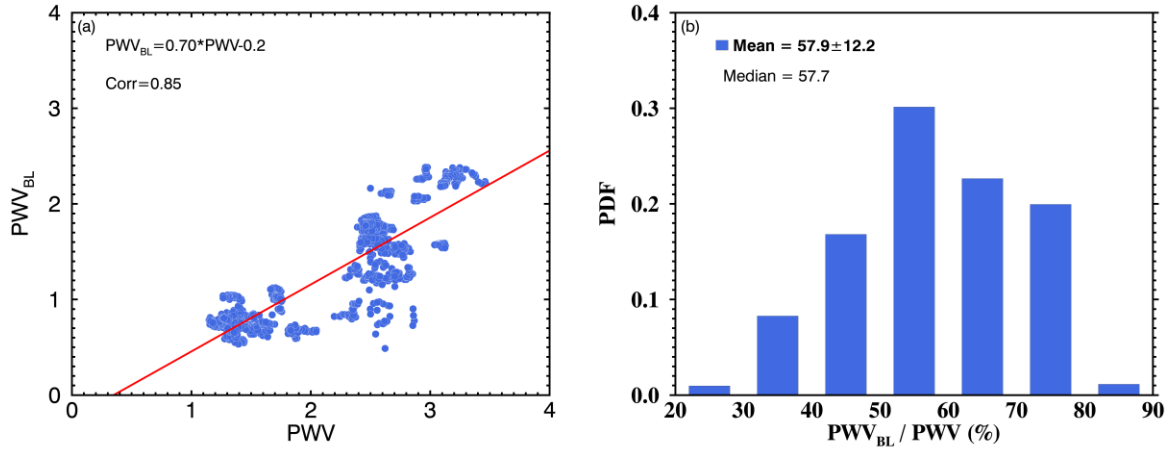


Figure S1. (a) Scatterplot of PWV versus PWV_{BL} ; and (b) distribution of the percentage ratio of PWV_{BL}/PWV .

- Not enough information is given about how the vertical velocity variance TKE_w is calculated. Is it a PBL average? A Doppler lidar column-deep average? Column max. value? And what Doppler lidar product are you using to get variance? The standard 10-minute integration? The median value seems low for surface-coupled stratocumulus cases. Are you evaluating any decoupled cases? There is also a diurnal and season cycle of turbulence at this site (at least, when sampling an undisturbed marine airmass; see more below), which may also be affecting your statistics.

In this study, the vertical component of the turbulence kinetic energy (TKE_w) are used, which is defined as:

$$TKE_w = \frac{1}{2} \overline{(w')^2}, \quad (2)$$

where the $(w')^2$ is the variance of vertical velocity measured from the Doppler lidar standard 10-min integration, which collected in the Doppler Lidar Vertical Velocity Statistics Value-Added Product (Newson et al., 2019). The noise correction has been applied to reduce the uncertainty of the variance to ~10% (Hogan et al., 2009; Pearson et al., 2009). In this study, the mean value of TKE_w in the sub-cloud

234 boundary layer proportion of the Doppler lidar range is used, and the data temporal resolution is further
235 downscaled to 5-min for temporal collocation purposes.

236 The description of TKE_w above has been added to the section 2.2 of the revised manuscript.

237

238 We have also included the decoupling index (D_i) given by: $D_i = (z_b - z_{LCL})/z_b$, where the z_{LCL}
239 is the lifting condensation level calculated analytically following the method in Romp (2017), with an
240 uncertainty of around 5 m. The surface temperature, pressure, relative humidity, and mass fraction of
241 water vapor that used in the z_{LCL} calculation, as long as the vector-averaged wind directions (in 360°
242 coordinate) over the ENA site are obtained from the ARM surface meteorology systems (ARM MET
243 handbook, 2011).

244 In this study, we are trying to examine the environmental effects on ACI_r under the diverse
245 conditions and whether the ACI_r can be distinguished by them, so that we did not have prior selection on
246 any particular environmental factors (except only the non-precipitating stratiform cloud cases), and thus
247 the samples including strongly decoupled, moderate-to-loosely decoupled and coupled MBL conditions.

248 From the PCA, the TKE_w has been found to be strongly positively correlated with $W_{dir,NS}$ and
249 negatively correlated with D_i , which means the values of TKE_w already account for the co-variabilities
250 in these variables. Therefore, treating TKE_w as the sorting variables would lead to a more physical
251 process-orientated assessment. And the corresponding discussion is revised in section 3.5.2 of the revised
252 manuscript.

253

254 •Have you controlled for wind direction in your analysis? It has been shown that there is an island
255 effect when the surface wind is from the island (e.g., Zheng, Rosenfeld and Li 2016). Overland
256 flow affects boundary layer turbulence and may also impact surface fluxes, PBL depth and
257 CCN composition.

258 We have considered the potential impact of the wind direction on the boundary layer turbulence,
259 and added to the PCA. In addition, the following summary on the island effects has been added to section
260 3.4 of the revised manuscript:

261 In Fig. 4, both TKE_w and $W_{dir,NS}$ vectors are located in the same quadrant (positive in both PC1
262 and PC2) and close to each other with a small degree of an acute angle, which means the TKE_w are
263 strongly correlated with the $W_{dir,NS}$. When the surface wind is coming from the north side of the island,

264 the topographic lifting effect of the cliff would induce additional updraft over the ENA site (Zheng et al.,
265 2016), so that the wind closer to the northerly wind (larger $W_{dir,NS}$) is more correlated with higher TKE_w .
266 Therefore, the values of TKE_w already account for the co-variation of TKE_w and $W_{dir,NS}$.

267

268 •How much does LTS tell us at a site like ENA, and what physical motivation do you have for
269 including it as a sorting variable? I always envision LTS as having the most meaning in the
270 subtropical eastern boundary current (EBC) areas, i.e., northeast/southeast Pacific and
271 southeast Atlantic. The Azores are more of a mixed subtropical/midlatitude site that has much
272 warmer SST than in the traditional EBC areas where MBL clouds are studied, and much of the
273 cloud cover at ENA occurs in transient postfrontal subsidence vs. longer-lasting large-scale
274 subsidence where the spatial gradient (of both subsidence and SST) matters more in defining
275 cloud type transitions.

276 We agree with your comment that the LTS might not be a feasible variable to use over ENA site,
277 we included the LTS as it is orthogonal to the TKE_w from the PCA and thus can be treated as
278 independence. We have added the relative discussion in section 3.5.2 of the revised manuscript:

279 Combining LTS and PWV_{BL} as sorting variables, the ACI_r values for four regimes are shown in
280 Fig. S4. The ACI_r differences between low and high PWV_{BL} regimes are still retained. In the low PWV_{BL}
281 regime, the ACI_r values are limited to 0.016 and 0.056 for low and high LTS regimes, respectively. In
282 the high PWV_{BL} regime, the ACI_r values are 0.150 and 0.171 for low and high LTS regimes, respectively,
283 which is about 3-5 times greater than those in low PWV_{BL} regime. However, the ACI_r in different LTS
284 regimes cannot be distinctly differentiated (ACI_r differences between LTS regimes are ~ 0.02 and ~ 0.04),
285 and the main difference in ACI_r are still induced by the PWV_{BL} . Owing to the location of the ENA site
286 where it locates near the boundary of mid-latitude and subtropical climate regimes, the MBL clouds over
287 the ENA are found to be often under the influences of cold fronts associated with mid-latitude cyclones,
288 where the cloud evolutions are subject to the combine effects of post-frontal and large-scale subsidence
289 (Wood et al., 2015; Zheng et al., 2020; Wang et al., 2021). Therefore, over the ENA, although the spatial
290 gradient of LTS is studied to be associated with the production of MBL turbulence and the change in
291 wind direction (Wu et al., 2017), the LTS value itself is examined to has a weak impact on the aerosol-
292 cloud interaction from this study.

- For arguments you make about the relationship between entrainment, collision-coalescence and number concentration, it is problematic that your retrieval assumes constant N_c throughout the cloud layer. When entrainment-induced evaporation and/or collision-coalescence are active, this assumption is broken. In general, I don't understand your argument that entrainment is a sink of N_c .

The Wu et al. (2020a) retrieval works as separating the reflectivity to the contributions of cloud (Z_c) and drizzle, the cloud procedure assumes an initial guess of the representative layer-mean N_c based on the climatology over ENA sites (Dong et al., 2014), and such allows the first guess of the vertical profile of LWC based on N_c and Z_c , and then constrains back the N_c and LWC using the LWP from MWR, finally output r_e (Fig.3 in Wu et al., 2020a). Therefore, the final retrieved N_c is updated to in response to the cloud microphysical processes within this time-step. From the aircraft in-situ measurements during the ACE-ENA, we used the in-situ measurement during ACE-ENA to validate the retrieval outputs and found that the observed N_c profile is near-constant in middle part of the cloud, with the signal of entrainment-induced depletion near the cloud top, even in the drizzling cloud where the collision-coalescence processes are more active (Wu et al., 2020a). However, it is hard and beyond the scope of the ground-based retrieval to compare the vertical dependency of depletion rate within one time-step. Therefore, as the retrieval currently work as representing the layer-mean information from the given time-step, the preferred method in this study is to compare N_c at different times, where in this case are the adiabatic versus sub-adiabatic conditions which hence yields different N_c that we retrieved from the ground-based snapshot perspective. From the PCA and binning analysis, the effect of cloud adiabaticities on CCN- N_c conversions may shed light on interpreting the aerosol-cloud interaction under different environmental effects.

We have added the above discussion in section 3.5.1 of the revised manuscript.

- High CCN events at ENA are not only from North America. They have also been traced to North Africa and Europe.

The corresponding sentence is changed to 'A few instances of aerosol intrusions (~3%) with higher $N_{CCN,0.2\%}$ were likely a result of continental air mass transport from North America, Europe, and Africa (Logan et al., 2014; Wang et al., 2020).'

323
324
325
326
327
328
329
330
331
332
333
334
335
336
337
338
339
340
341
342
343
344
345
346
347
348
349
350
351
352

References.

Wu, P., Dong, X., Xi, B., Tian, J. and Ward, D. M.: Profiles of MBL Cloud and Drizzle Microphysical Properties Retrieved From Ground-Based Observations and Validated by Aircraft In Situ Measurements Over the Azores, *J. Geophys. Res. Atmos.*, doi:10.1029/2019JD032205, 2020a.

Zheng, Y., Rosenfeld, D. and Li, Z.: Quantifying cloud base updraft speeds of marine stratocumulus from cloud top radiative cooling, *Geophys. Res. Lett.*, doi:10.1002/2016GL071185, 2016.

Zheng, Y., Rosenfeld, D. and Li, Z.: A More General Paradigm for Understanding the Decoupling of Stratocumulus-Topped Boundary Layers: The Importance of Horizontal Temperature Advection, *Geophys. Res. Lett.*, doi:10.1029/2020GL087697, 2020.

Response to Reviewer #3

We appreciate your time for carefully reviewing our manuscript. We would like to thank you for the constructive comments and suggestions, which encourage and help us to improve the manuscript. The manuscript has been revised accordingly. In the response below, your comments are provided in black text and our responses are provided in blue text.

Response:

The authors analyze the impact of the environment on the aerosol-cloud interactions (ACI) from ground observations over the eastern north Atlantic. They find that both lower-tropospheric stability and turbulent kinetic energy influence the connection between water vapor, cloud-microphysics, and subsequently ACI. For instance, they find that higher lower-tropospheric stability leads to higher cloud drop concentrations and ACI.

Overall, I think this paper is both well thought out and written. However, I do have a number of issues that I would appreciate clarification on. Note that, even though I split my comments between major and minor, this is more of just a distinction between general and technical comments. Therefore, I recommend publication once these comments are addressed.

Major:

Line 147: Is LTS the most appropriate variable to use over the northeast Atlantic, considering the much larger influence of midlatitude cyclones compared to subtropical regions?

We agree with your comment and the other reviewer's comment that the LTS might not be a feasible variable to use over ENA site, and thus we have added the relative discussion in section 3.5.2 of the revised manuscript:

Combining LTS and PWV_{BL} as sorting variables, the ACI_r values for four regimes are shown in Fig. S4. The ACI_r differences between low and high PWV_{BL} regimes are still retained. In the low PWV_{BL} regime, the ACI_r values are limited to 0.016 and 0.056 for low and high LTS regimes, respectively. In the high PWV_{BL} regime, the ACI_r values are 0.150 and 0.171 for low and high LTS regimes, respectively, which is about 3-5 times greater than those in low PWV_{BL} regime. However, the ACI_r in different LTS regimes cannot be distinctly differentiated (ACI_r differences between LTS regimes are ~ 0.02 and ~ 0.04), and the main difference in ACI_r are still induced by the PWV_{BL} . Owing to the location of the ENA site where it locates near the boundary of mid-latitude and subtropical climate regimes, the MBL clouds over the ENA are found to be often under the influences of cold fronts associated with mid-latitude cyclones,

385 where the cloud evolutions are subject to the combine effects of post-frontal and large-scale subsidence
386 (Wood et al., 2015; Zheng et al., 2020; Wang et al., 2021). Therefore, over the ENA, although the spatial
387 gradient of LTS is studied to be associated with the production of MBL turbulence and the change in
388 wind direction (Wu et al., 2017), the LTS value itself is examined to has a weak impact on the aerosol-
389 cloud interaction from this study.

390

391 Line 171: How many potential non-precipitating cloud cases were there, and do your results suggest that
392 most MBL clouds produce precip over the northeast Atlantic?

393 During the study period we found 20 valid non-precipitating single-layer low cloud case that fit in our
394 criteria and also lasting at least longer than 2 hours. And yes, our results support the previous study that
395 over the ENA site, the annual mean drizzle frequency is 55%, with 70% in winter and 45% in summer
396 (Wu et al., 2020).

397 Line 193: You could highlight that the median LTS of 19.1 K is close to the value (18.55 K) used by
398 prior studies to separate stratocumulus from shallow cumulus.

399 The result from prior study is highlighted as follows:

400 Note that the median LTS of 19.1 K in this study is close to the separation threshold of 18.55K suggested
401 by prior studies to distinguish the marine stratocumulus from a global assessment of marine shallow
402 cumulus clouds (Smalley and Rapp, 2020).

403 Line 226: You compare the logarithmic ratio that you find to other studies, but I don't understand what
404 it actually means.

405 The ratio reflects the relative conversion efficiency of cloud droplets from the CCN, regardless of the
406 water vapor availabilities. Theoretically it has the boundaries of 0 - 1, where the lower bound means no
407 change of N_c with N_{CCN} , and the upper bound indicates a linear relationship that every CCN would result
408 in one cloud droplet. Our result is comparable with the previous studies that also targeting the MBL
409 stratiform clouds, indicates a certain similarity of the bulk cloud microphysical responses with respect to
410 aerosol intrusion in those type of cloud and over different marine environments, further support that the
411 assessment in this study is valid.

412 The discussion above is added in section 3.2 in the revised manuscript.

413 Figures 5 - 7: There doesn't appear to be much of a trend in the scatter plots, so what is the R^2 value for
414 these regressions? Maybe this could be fixed by constraining your axes to closer to the limits of your
415 datapoints?

416 In the revise manuscript, we changed to use the sub-cloud PWV_{BL} in sorting the data, as suggested by
417 reviewer #2. We have constrained the plotting axes to be closer to the data points. Since the values of
418 ACI_r have a theoretical upper bound of 0.33 (McComiskey et al., 2009), so even the largest ACI_r will
419 probably not showing a steep trend in the scatterplot. However, the slopes of regression can be
420 distinguished, all linear regressions for those groups of data have been tested by two-tailed T statistic
421 and pass the 95% significant level.

422 Minor:

423 Line 77: "relatively shallower" should be "relatively shallow"

424 The word is changed to 'shallow'.

425 Line 78: I think "and is prone to" should be and "are prone to"

426 It is changed to 'are prone to'.

427 Line 80: "marine boundary layer maintained by" should be "marine boundary layer which is maintained
428 by"

429 The 'which is' is added to the sentence.

430 line 85: "regime of active coalescence process" should either be "regime of the active coalescence
431 process" or "regime of active coalescence"

432 It is changed to 'regime of active coalescence'.

433 line 106: "particularly disentangling" should be "particularly by disentangling"

434 It is changed to 'particularly by disentangling'.

435 line 121: "operates at 910 nm laser beam" doesn't make sense, and maybe could be "operates at 910nm"

436 It is changed to 'operates at 910 nm'.

437 line 159: "from Doppler lidar" should either be "from a Dopplar lidar" or "from the Dopplar lidar"

438 It is changed to 'from the Doppler lidar'.

439 line 183: "lay" should be "lie"

440 It is changed to 'lie'.

441 line 388: Unless I missed something why is Figure 5b discussed before Figure 5a, could you just flip

442 those subpanels?

443 The figure subpanel is flipped.

444 Figure 1: This may just be my printout, but the median dashed lines are difficult to see. Could you use a

445 thicker line or a different color?

446 The median value is now displayed directly on each subpanel in Figure 1.

447

448 **Reference:**

449 McComiskey, A, Feingold, G., Frisch, A. S., Turner, D. D., Miller, M., Chiu, J. C., Min, Q. and Ogren,

450 J.: An assessment of aerosol-cloud interactions in marine stratus clouds based on surface remote

451 sensing, J. Geophys. Res., 114, D09203, doi:10.1029/2008JD011006, 2009.

452 Smalley, K. M. and Rapp, A. D.: The role of cloud size and environmental moisture in shallow cumulus

453 precipitation, J. Appl. Meteorol. Climatol., doi:10.1175/JAMC-D-19-0145.1, 2020.

454 Wu, P., Dong, X. and Xi, B.: A climatology of marine boundary layer cloud and drizzle properties

455 derived from ground-based observations over the azores, J. Clim., doi:10.1175/JCLI-D-20-0272.1,

456 2020.

457

458

459

Revised Version

Environmental Effects on Aerosol-Cloud Interaction in non-precipitating MBL Clouds over the Eastern North Atlantic

Xiaojian Zheng¹, Baike Xi¹, Xiquan Dong¹, Peng Wu², Yuan Wang^{3,4} and Timothy Logan⁵

¹Department of Hydrology and Atmospheric Sciences, University of Arizona, Tucson, AZ, USA

²Pacific Northwest National Laboratory, Richland, WA, USA

³Division of Geological and Planetary Sciences, California Institute of Technology, Pasadena, CA, USA

⁴Jet Propulsion Laboratory, California Institute of Technology, Pasadena, CA, USA

⁵Department of Atmospheric Sciences, Texas A&M University, College Station, TX, USA

Correspondence: Baike Xi (baikex@arizona.edu)

Abstract. Over the eastern north Atlantic (ENA) ocean, a total of 20 non-precipitating single-layer marine boundary layer (MBL) stratus and stratocumulus cloud cases are selected to investigate the impacts of the environmental variables on the aerosol-cloud interaction (ACI_r) using the ground-based measurements from the Department of Energy Atmospheric Radiation Measurement (ARM) facility at the ENA site during 2016 – 2018. The ACI_r represents the relative change of cloud-droplet effective radius r_e with respect to the relative change of cloud condensation nuclei (CCN) number concentration at 0.2% supersaturation ($N_{CCN,0.2\%}$) in the water vapor stratified environment. The ACI_r values vary from -0.01 to 0.22 with increasing sub-cloud boundary layer precipitable water vapor (PWV_{BL}) conditions, indicating that r_e is more sensitive to the CCN loading under sufficient water vapor supply, owing to the combined effect of enhanced condensational growth and coalescence processes associated with higher N_c and PWV_{BL} . The principal component analysis shows that the most pronounced pattern during the selected cases is the co-variations of the MBL conditions characterized by the vertical component of turbulence kinetic energy (TKE_w), decoupling index (D_i) and PWV_{BL} . The environmental effects on ACI_r emerge after the data are stratified into different TKE_w regimes. The ACI_r values, under both relatively lower and higher PWV_{BL} conditions, increase more than double from the low TKE_w to high TKE_w regime. It can be explained by the fact that stronger boundary layer turbulence maintains a well-

mixed MBL, strengthening the connection between cloud microphysical properties and underneath CCN and moisture sources. With sufficient water vapor and low CCN loading, the active coalescence process broadens the cloud droplet size spectra, and consequently results in an enlargement of r_e . The enhanced N_c conversion and condensational growth induced by more intrusions of CCN effectively decrease r_e , which jointly presents as the increased ACI_r . This study examines the importance of environmental effects on the ACI_r assessments and provides observational constraints to future model evaluations on aerosol-cloud interactions.

1. Introduction

Clouds are one of the most important parts of the Earth's climate system. They can impact the global climate by modulating the radiative balance in the atmosphere. Moreover, the radiative effects of cloud adjustments due to aerosols remain one of the largest uncertainties in climate modeling (IPCC, 2013). Over the oceanic area, the lower troposphere is dominated by marine boundary layer (MBL) clouds. MBL clouds can persistently reflect the solar radiation by their long-lasting nature maintained by cloud-top radiative cooling, and therefore act as a major modulator of the Earth radiative budget (Seinfeld et al., 2016). The climatic importance of MBL cloud radiative properties is primarily induced by cloud microphysical properties, namely the cloud-droplet number concentration (N_c), and effective radius (r_e), and has been intensively investigated by many researchers (Garrett and Zhao, 2006; Rosenfeld, 2007; Wood et al., 2015; Seinfeld et al., 2016). The ambient aerosol conditions can influence these cloud microphysical properties via the aerosol-cloud interaction (ACI). Compared to the clean regions, clouds under the regions having relatively higher below-cloud aerosol concentrations exhibited more small cloud droplets (reduced r_e and increased N_c) and enhanced both cloud liquid water contents and optical depths (McComiskey et al., 2009; Chen et al., 2014; Wang et al., 2018). The changes of MBL cloud microphysical properties induced by aerosols have been investigated from previous studies using in-situ measurements, ground- and satellite-based observations, and model simulations in multiple oceanic areas such as the eastern Pacific and eastern Atlantic (Twohy et al., 2005; Lu et al., 2007; Hill et al., 2009; Costantino and Bréon, 2010; Mann et al., 2014; Dong et al., 2015; Diamond et al., 2018; Yang et al., 2019; Zhao et al., 2019; Wang et al., 2020).

The assessments of ACI, particularly using ground-based remote sensing, vary in terms of the quantitative values, which represent the different cloud susceptibilities to aerosol loadings. Owing to the numerous approaches in assessing the ACI, such as the spatial and temporal scales, N_c and r_e retrieval

methods, and more importantly, the different aerosol proxies used in the ACI quantification, different ACI results could be achieved. For example, the studies using total aerosol number concentration and aerosol scattering/extinction coefficients to represent the aerosol loadings would result in relatively lower ACI values (Pandithurai et al., 2009; Liu et al., 2016). This is primarily attributed to the inclusion of aerosol species with different abilities to activate, which is determined by their physicochemical properties, and thus will cause non-negligible uncertainties in capturing the information of aerosol intrusion to the cloud (Feingold et al. 2006; Logan et al., 2014). While some studies found relatively higher ACI values using cloud condensation nuclei (CCN) number concentration (N_{CCN}), presumably due to the fact that CCN represents the portion of aerosols that can be activated and possesses the potential ability to further grow into cloud droplets, this favorably yields a more straightforward assessment of ACI (McComiskey et al., 2009; Qiu et al., 2017; Zheng et al., 2020). It is noteworthy that the ACI variations have been found to have both increasing and decreasing trends in response to changing environmental water availability (Martin et al., 2004; Kim et al., 2008; McComiskey et al., 2009; Pandithurai et al., 2009; Martin et al., 2011; Liu et al., 2016; Zheng et al., 2020). Although these contradicting results have been postulated due to multiple factors such as cloud adiabaticity, condensational growth, collision coalescence, and atmospheric thermodynamics and dynamics, the underlying mechanisms in altering the ACI and causing the uncertainties in the ACI assessments remain unclear. Therefore, further studies are necessary (Fan et al., 2016; Feingold and McComiskey, 2016; Seinfeld et al., 2016).

The Eastern North Atlantic (ENA) is a remote oceanic region that features persistent but diverse subtropical MBL clouds, owing to complex meteorological influences from the semi-permanent Azores High and prevailing large-scale subsidence (Wood et al., 2015). The ENA has become a favorable region to study the aerosol indirect effects on MBL clouds under a relatively clean environment with occasional intrusions of long-range transport of continental air mass (Logan et al., 2014; Wang et al., 2020). The atmospheric radiation measurement (ARM) program established the ENA permanent observatory site on the northern edge of Graciosa Island, Azores, in 2013, which continuously provides comprehensive measurements of the atmosphere, radiation, cloud, and aerosol from ground-based observation instruments. Owing to the location of the site, where sits in between the boundaries of mid-latitude and subtropical regimes, the ENA is under the mixed influence of diverse meteorological conditions. So that in terms of the aerosol influence on the cloud properties, the roles of meteorological factors on cloud formation and development are not negligible and hence are being explored in this study. The large-scale thermodynamic variables of the lower troposphere are widely used, such as the lower tropospheric stability (LTS), where the higher LTS values are found to be associated with a relatively shallow and

557 well-mixed marine boundary layer, and are prone to stratiform cloud formations with higher cloud
558 fractions (Klein and Hartmann, 1993; Wood, 2012; Wood and Bretherton, 2006; Yue et al., 2011;
559 Rosenfeld et al., 2019), especially over the subtropical ocean such as the southeast Atlantic. Over the
560 ENA site, the spatial gradient of the LTS has been studied to be associated with the contribution terms
561 of MBL turbulence and the wind directional change (Wu et al., 2017).

562 In the cloud-topped MBL which is maintained by cloud-top radiative cooling, the buoyancy
563 generations and shears contribute most to the turbulence kinetic energy (TKE) production (Nicholls,
564 1984; Hogan et al., 2009), where the intensity of turbulence denotes the coupling of MBL clouds to the
565 below-cloud boundary layer. In terms of the cloud droplet growing process, especially in a clean
566 environment with low N_{CCN} below the cloud layer, the cloud droplets at the cloud base experience rapid
567 growth via the diffusion of water vapor, and subsequently enter the regime of active coalescence
568 (Rosenfeld and Woodley, 2003; Martins et al., 2011). The intensive turbulence effectively modulates the
569 cloud droplet growth by strengthening the coalescence process and the cloud cycling (Feingold et al.,
570 1996, 1999; Pawlowska et al., 2006). And particularly giving the unique topography of the Graciosa
571 Island, the island effect would cause disturbances on the updraft and hence impact the MBL turbulence,
572 depending on the surface wind directions (Zheng et al., 2016). The environmental effects on the MBL
573 cloud formation and development processes and cloud microphysical properties have been widely
574 implemented and considered in climate modeling (Medeiros and Stevens, 2011; West et al., 2014; Zhang
575 et al., 2016). Thus, it is important to provide observational constraints on the environmental effects. The
576 assessment of ACI from the ground-based perspective highly relies on the sensitivities of cloud droplet
577 number concentrations and size distribution to the changing of below-cloud CCN loadings. Hence,
578 studying the relationship between the environmental effect and the MBL cloud microphysical responses
579 is a nontrivial task.

580 In this study, we target the non-precipitating single-layer MBL stratus and stratocumulus clouds
581 during the period between September 2016 and May 2018 and examine the role of thermodynamical and
582 dynamical variables on ACIs. This study aims to advance the understanding of ACI by disentangling
583 the environmental effects and providing observational constraints on quantifying the ACI when modeling
584 aerosol effects on MBL clouds. The ground-based observations and retrievals, and the reanalysis are
585 introduced in section 2. Section 3 describes the aerosol, cloud and meteorological properties, and the
586 variations of cloud microphysical properties under different environmental regimes. Moreover, the ACIs
587 under given water vapor conditions and the roles of environmental effects on ACI are discussed in
588 Section 3. The conclusion of the key findings and the future work are presented in section 4.

589

590 2. Data and methods

591 2.1 Cloud and aerosol properties

592 The cloud boundaries at the ARM ENA site are primarily determined by the ARM Active Remotely-
593 Sensed Cloud Locations (ARSCL) product, which is a combination of data detected by multiple active
594 remote-sensing instruments, including the Ka-band ARM Zenith Radar (KAZR) and laser ceilometer.
595 The KAZR has an operating frequency at 35 GHz and is sensitive in cloud detection with very minimum
596 attenuation up to the cloud top height (Widener et al., 2012). The temporal and vertical resolutions of
597 KAZR reflectivity are 4 seconds and 30 m, respectively. The ceilometer operates at 910 nm and its
598 attenuated backscatter data can be converted to the cloud base height up to 7.7 km with an uncertainty
599 of ~10 m (Morris, 2016). Combining both KAZR and ceilometer measurements, the cloud base (z_b) and
600 top (z_t) heights can be identified accordingly. The single-layer low cloud is defined as having a cloud
601 top height lower than 3 km, with no additional cloud layer in the atmosphere above (Xi et al., 2010).

602 The cloud microphysical properties are retrieved from a combination of ground-based observations,
603 including KAZR, ceilometer, and microwave radiometer. The detailed retrieval methods and procedures
604 are described in Wu et al. (2020a). The retrieved cloud microphysical properties, both in time series and
605 vertical profiles, have been validated using the collocated aircraft in-situ measurements during the
606 Aerosol and Cloud Experiments in the Eastern North Atlantic field campaign (ACE-ENA). The retrieval
607 uncertainties are estimated to be ~15% for cloud droplet effective radius (r_e), ~35% for cloud droplet
608 number concentration (N_c), and ~30% for the cloud liquid water content (LWC) (Wu et al., 2020a).
609 Furthermore, the cloud adiabaticity is calculated using the retrieved in-cloud vertical profile of LWC and
610 the adiabatic LWC_{ad} . The LWC_{ad} is given by $LWC_{ad}(z) = \Gamma_{ad}(z - z_b)$, following the method in Wu et
611 al. (2020b), where Γ_{ad} denotes the linear increase of LWC with height under an ideal adiabatic condition
612 (Wood, 2005). The cloud adiabaticity (f_{ad}) is defined as the ratio of LWC to LWC_{ad} .

613 The surface CCN number concentrations (N_{CCN}) are measured by the CCN-100 (single-column)
614 counter. Since the supersaturation (SS) levels are set to cycling between 0.10% and 1.10% approximately
615 within one hour, N_{CCN} under a relatively stable supersaturation level has to be carefully calculated to rule
616 out the impact of supersaturation on N_{CCN} . This study adopts the interpolation method given by $N_{CCN} =$
617 cSS^k (Twomey, 1959), where parameters c and k are fitted by a power-law function for every periodic
618 cycle. In this study, the supersaturation level of 0.2% is used because it represents typical supersaturation
619 conditions of boundary-layer stratiform clouds (Hudson and Noble, 2013; Logan et al., 2014; Wood et
620 al., 2015; Siebert et al., 2021), and N_{CCN} at 0.2% supersaturation (hereafter $N_{CCN,0.2\%}$) is interpolated to
621 5-min temporal resolution.

622

623 **2.2 Environmental conditions and cloud case selections**

624 The integrated precipitable water vapor (PWV) is obtained from a 3-channel microwave radiometer
 625 (MWR3C), which operates at three frequency channels of 23.834, 30, and 89 GHz. The uncertainty of
 626 PWV is estimated to be ~ 0.03 cm (Cadeddu et al., 2013). To capture the information of MBL water vapor
 627 more accurately, the sub-cloud boundary layer integrated precipitable water vapor (PWV_{BL}) is calculated
 628 using the interpolated sounding product following:

$$629 \text{PWV}_{\text{BL}} = \frac{1}{\rho_w} \sum (z_{i+1} - z_i) * (\rho_{v,i+1} + \rho_{v,i}) / 2, \quad (1)$$

630 where the ρ_w is the liquid water density and the ρ_v is the water vapor density collected from the
 631 Interpolated Sounding and Gridded Sounding Value-Added Products (Toto and Jensen, 2016), the
 632 subscripts i and $i + 1$ represent the bottom and top of each interpolated sounding height layer. Both
 633 PWV and PWV_{BL} are temporally collocated to 5-min resolution and plotted against each other in Fig.
 634 S1a to test the contribution of PWV_{BL} to the PWV. The Pearson correlation coefficient of 0.85 shows
 635 that the PWV_{BL} are strongly positively correlated with the PWV, while the distribution of the percentage
 636 ratio of PWV_{BL} to PWV (Fig. S1b) indicates that, on average, the PWV_{BL} contribute to $\sim 58\%$ of the
 637 PWV. Considering the cloud-topped MBL, the majority of cases ($\sim 74\%$) associate with a relatively moist
 638 boundary layer compared to the amount of water vapor in the free troposphere, where the PWV_{BL} already
 639 contributed over 50% of the total column PWV. In contrast, only $\sim 9\%$ of cloud samples occur under a
 640 relatively dry boundary layer and moist free troposphere, where PWV_{BL} contributions are less than 40%.
 641 In general, the PWV can well capture the variation of the PWV_{BL}. In the rest of the study, the PWV_{BL}
 642 are used, as it represents the sub-cloud boundary layer water vapor availabilities which are more closely
 643 related to the MBL cloud processes.

644 The LTS parameter is used as a proxy of large-scale thermodynamic structure and is defined as the
 645 difference between the potential temperature at 700 hPa and surface ($\theta_{700} - \theta_{sf}$). The LTS values are
 646 calculated from European Centre for Medium-Range Weather Forecasts (ECMWF) model outputs of
 647 potential temperature, by averaging over a grid box of $0.56^\circ \times 0.56^\circ$ centered at the ENA site. To match
 648 the temporal resolutions of the other variables, the original 1-hour LTS data are downsampled to 5-min
 649 under the assumption that the large-scale forcing would not have significant changes within an hour.

650 The boundary layer decoupling condition is represented by the decoupling index (D_i), which is
 651 given by $D_i = (z_b - z_{LCL})/z_b$, where the z_{LCL} is the lifting condensation level calculated analytically
 652 following the method in Romp (2017), with an uncertainty of around 5 m. The surface temperature,

653 pressure, relative humidity, and mass fraction of water vapor that used in the z_{LCL} calculation, as long as
654 the vector-averaged wind directions (in 360° coordinate) over the ENA site are obtained from the ARM
655 surface meteorology systems (ARM MET handbook, 2011).

656 As for the boundary layer dynamics, the higher-order moments of vertical velocity are widely used
657 in different model parameterization practices, such as higher-order turbulence closure and probability
658 density function methods (Lappen and Randall, 2001; Zhu and Zuidema, 2009; Ghate et al., 2010). The
659 vertical velocity variance can be used to represent the turbulence intensity in the below-cloud boundary
660 layer (Feingold et al., 1999). In this study, the vertical component of the turbulence kinetic energy (TKE_w)
661 are used, which is defined as:

$$662 \quad TKE_w = \frac{1}{2} \overline{(w')^2}, \quad (2)$$

663 where the $(w')^2$ is the variance of vertical velocity measured from the Doppler lidar standard 10-min
664 integration, which is collected in the Doppler Lidar Vertical Velocity Statistics Value-Added Product
665 (Newson et al., 2019). The noise correction has been applied to reduce the uncertainty of the variance to
666 ~10% (Hogan et al., 2009; Pearson et al., 2009). In this study, the mean value of TKE_w in the sub-cloud
667 boundary layer proportion of the Doppler lidar range is used, and the data temporal resolution is further
668 downsampled to 5-min for temporal collocation purposes.

669 In this study, the non-precipitating cloud periods are determined when the KAZR reflectivity at the
670 ceilometer-detected cloud base height range does not exceed -37 dBZ (Wu et al., 2015, 2020b), which
671 extensively rules out the wet-scavenging depletion on below-cloud CCN (Wood, 2006) and ensures the
672 accuracy in capturing the below-cloud CCN loadings. Both retrieved cloud microphysical properties and
673 CCN data are available from September 2016 to May 2018 and confine this period in this study.

674

675 **3. Result and Discussion**

676 **3.1 Aerosol, cloud, and meteorological properties of selected cloud cases**

677 A total of 20 non-precipitating cloud cases are selected in this study, with the detailed time periods
678 listed in Table 1, including 1143 samples with temporal resolution of 5-min, which corresponds to ~95
679 hours. Among the selected cases, there are three, eight, five, and four cases for Spring, Summer, Fall,
680 and Winter seasons, respectively. MBL clouds often produce precipitation in the form of drizzle (Wood
681 2012, Wu et al., 2015, 2020b). A recent study of the seasonal variation of the drizzling frequencies (Wu
682 et al., 2020b) showed that the MBL clouds in the cold months (Oct-Mar) have the highest drizzling
683 frequency of the year (~70%), while the clouds in the warm months (Apr-Sept) are found to have a lower
684 chance of drizzling (~45%). Therefore, the selection of a non-precipitating single-layer low cloud case

685 that lasts at least 2 hours is limited, with only 6 cases found in the cold months and 14 cases found during
686 the warm months.

687 The probability distribution functions (PDFs) of the aerosol and cloud properties, and the
688 environmental conditions for the selected cases are shown in Fig. 1. The PDF of $N_{CCN,0.2\%}$ presents a
689 normal distribution with a mean value of 215 cm^{-3} and median value of 217 cm^{-3} . About 97% of the
690 $N_{CCN,0.2\%}$ samples lie below 350 cm^{-3} and represents a relatively clean environment (Logan et al., 2014,
691 2018). A few instances of aerosol intrusions ($\sim 3\%$) with higher $N_{CCN,0.2\%}$ were likely a result of
692 continental air mass transport from North America, Europe, and Africa (Logan et al., 2014; Wang et al.,
693 2020). As for the cloud microphysical properties, the cloud-layer mean N_c and r_e (Fig. 1b and 1c) are
694 also both normally distributed with median values close to the mean values. The majority of the N_c
695 values ($\sim 91\%$) are lower than 125 cm^{-3} with a mean value of 86 cm^{-3} , and the r_e distribution peaks at
696 $9 - 11 \text{ }\mu\text{m}$ with a mean value of $10.1 \text{ }\mu\text{m}$. Both N_c and r_e values fall in the typical ranges of the non-
697 precipitating MBL cloud characteristics over the ENA site (Dong et al., 2014; Wu et al., 2020b). The
698 distribution of f_{ad} is slightly skewed to the left with a median value of 0.66 (Fig. 1d), indicates that the
699 bulk of cloud samples are close to adiabatic environments, while the left tail denotes a wide range of
700 cloud sub-adiabaticities, which allows us to investigate the role of cloud adiabaticities on the cloud
701 microphysical variations.

702 For all selected cases, the LTS, which represents the large-scale thermodynamic structure, is
703 distributed bimodally across the range from 14K to 23K with mean and median values of 19.1K in Fig.
704 1e. A higher LTS magnitude represents a relatively stable environment and is favorable to the formation
705 of marine stratocumulus (Medeiros and Stevens, 2011; Gryspeerdt et al., 2016). Note that the median
706 LTS of 19.1 K in this study is close to the separation threshold of 18.55K suggested by prior studies to
707 distinguish the marine stratocumulus from a global assessment of marine shallow cumulus clouds
708 (Smalley and Rapp, 2020). Therefore, leveraging the demarcation line at 19.1K may allow us to
709 investigate the aerosol-cloud relationships under contrasting thermodynamic regimes. The PDF of D_i
710 parameter spreads widely with a median value of 0.34 for the selected cases (Fig. 1f), which provides an
711 opportunity to study the cloud sample behaviors under MBL conditions range from well-mixed to
712 decoupled. Higher D_i values indicate more decoupled MBL with weaker turbulence which cannot
713 sufficiently maintain the well-mixed MBL, while lower D_i values often associate with stronger
714 turbulence which maintains a coupled MBL (Jones et al., 2011). As an indicator of the below-cloud
715 boundary layer turbulence, the TKE_w values present a gamma distribution that is highly skewed to the
716 right (Fig. 1e), with a mean value of 0.11 and a median value of $0.08 \text{ m}^2\text{s}^{-2}$. About half of the cloud

717 samples are under relatively less turbulent environment (which is also implied by the higher half of D_t),
 718 suggesting weak connections between the cloud layer and the below-cloud boundary layer. The other
 719 half of the cloud samples, with relatively higher TKE_w values up to $0.4 \text{ m}^2/\text{s}^2$, imply tighter connections
 720 between cloud microphysical properties and below-cloud boundary layer accompanied by intensive
 721 turbulent conditions, which is favorable to enhance cloud droplet growth (Albrecht et al., 1995; Hogan
 722 et al., 2009; Ghate et al., 2010; West et al., 2014; Ghate and Cadetdu, 2019).

723 It is noteworthy that PWV_{BL} values exhibit a bimodal distribution with a median value of 1.2 cm
 724 (Fig. 1f). About 49% of the samples have their PWV_{BL} values in the range of 0.4 - 1.2 cm with the first
 725 peak in 0.6 - 0.8 cm, and 51% of the samples have PWV_{BL} values higher than 1.2 cm with a second peak
 726 in 1.6 - 1.8 cm, which may be due to the seasonal difference of the selected cases. Fig. S2 shows the
 727 seasonal variation of the PWV_{BL} from 2016 to 2018 when single-layered low clouds are present. The
 728 monthly PWV_{BL} values are as low as ~ 0.9 cm and remain nearly invariant from January through March,
 729 then increase to ~ 2.0 cm (doubled) in September, and decrease dramatically to the winter months. The
 730 selected cloud cases are distributed across the seasons, with $\sim 34\%$ of the samples occurring during the
 731 months with the lowest mean PWV_{BL} (Jan-Mar), while $\sim 43\%$ of the samples fall in the highest PWV_{BL}
 732 months (Jun-Sept). These two different PWV_{BL} regions will provide a great opportunity for us to further
 733 examine the ACI under relatively lower and higher water vapor conditions.

734 735 **3.2 Dependent of cloud microphysical properties on CCN and PWV_{BL}**

736 Figure 2 shows the cloud microphysical properties as a function of $N_{CCN,0.2\%}$ and PWV_{BL} for the
 737 samples from 20 selected cases. As illustrated in Fig. 2a, there is a statistically significant positive
 738 correlation ($R^2=0.9$) between $\ln(N_c)$ and $\ln(N_{CCN,0.2\%})$. The linear fit of $\ln(N_c)$ to $\ln(N_{CCN,0.2\%})$ is then
 739 mathematically transformed to a power-law fitting function of N_c to $N_{CCN,0.2\%}$, and plotted as dash lines
 740 in Fig. 2a. The power-law fitting indicates that 90.3% of the variation in binned $\ln(N_c)$ can be explained
 741 by the change in the binned $\ln(N_{CCN,0.2\%})$ and further suggests that with more available below-cloud
 742 CCN, higher number concentrations are expected. The logarithmic ratio $\partial \ln(N_c)/\partial \ln(N_{CCN,0.2\%})$ is
 743 computed to be 0.435 from our study. This ratio is very close to 0.48 found by McComiskey et al. (2009),
 744 who also used ground-based measurements to study the marine stratus clouds over the California coast.
 745 The logarithmic ratio (0.435) is also close to the result (0.458) of Lu et al. (2007) who used aircraft in-
 746 situ measured cloud droplet and accumulation mode aerosol number concentration for the marine stratus
 747 and stratocumulus clouds over the eastern Pacific Ocean. The ratio reflects the relative conversion
 748 efficiency of cloud droplets from the CCN, regardless of the water vapor availabilities. Theoretically, it

has the boundaries of 0 - 1, where the lower bound means no change of N_c with N_{CCN} , and the upper bound indicates a linear relationship that every CCN would result in one cloud droplet. Our result is comparable with the previous studies targeting the MBL stratiform clouds, indicating a certain similarity of the bulk cloud microphysical responses with respect to aerosol intrusion in those types of cloud and over different marine environments, further support that the assessment in this study is valid.

The PWV_{BL} values are represented as blue circles (larger one for higher PWV_{BL}) in Fig. 2a in order to study the role of water vapor availability on the $CCN-N_c$ conversion process. As demonstrated in Fig. 2a, the PWV_{BL} values almost mimic the increasing $N_{CCN,0.2\%}$ trend, which is also governed by the seasonal $N_{CCN,0.2\%}$ and the selected cloud cases. Fig. S3 shows the seasonal variation of $N_{CCN,0.2\%}$ from 2016 to 2018. It is noticeable that the monthly $N_{CCN,0.2\%}$ values, which mimic the monthly variation of PWV_{BL} , are much higher during warm months (May-Oct) than during cold months (Nov-Apr). This seasonal $N_{CCN,0.2\%}$ variation is also found in recent studies of MBL aerosol composition and number concentration. During the warm months, the below-cloud boundary layer is enriched by the accumulation mode of sulfate and organic particles via local generation and long-range transport induced by the semi-permanent Azores High, which are found to be hydrophilic and can be great CCN contributors (Wang et al., 2020; Zawadowicz et al., 2020; Zheng et al., 2018, 2020). Therefore, the coincidence of high $N_{CCN,0.2\%}$ and PWV_{BL} does not necessarily imply a physical relationship, but instead is the result of their similar seasonal trend. The potential co-variabilities between $N_{CCN,0.2\%}$ and PWV_{BL} , and hence the implication on the N_c variation will be further investigated in the latter section. When taking the PWV_{BL} into account, R^2 increases from 0.903 to 0.982, and this new relationship suggests that the co-variability between the binned $\ln(N_{CCN,0.2\%})$ and $\ln(PWV_{BL})$ are in a stronger correlation with the change in binned $\ln(N_c)$. Intuitively, if the $CCN-N_c$ relationship is primarily dominated by the diffusion of water vapor, more CCN and higher PWV_{BL} should result in a continuously increasing of N_c . However, the rapid increase of N_c (37 to 92 cm^{-3}) in the first half of $N_{CCN,0.2\%}$ bins ($<250 cm^{-3}$) does not happen in the second half of the $N_{CCN,0.2\%}$ bins ($>250 cm^{-3}$) where the slope of N_c increase (96 to 103 cm^{-3}) appears to be flattened for higher $N_{CCN,0.2\%}$ and PWV_{BL} bins. Furthermore, the joint power-law fitting of N_c (to $N_{CCN,0.2\%}$ and PWV_{BL}) appears to be constantly lower than the single power-law fitting of N_c (to $N_{CCN,0.2\%}$ solely) in each bin. The negative power of PWV_{BL} in this relationship suggests that PWV_{BL} might play a stabilization role in the diffusional growth process, which will be further analyzed in the following sections.

The relationship between r_e and $N_{CCN,0.2\%}$ is shown in Fig. 2b where there is no significant relationship between r_e with $N_{CCN,0.2\%}$ solely, given a near-zero slope and the low correlation coefficient

(fitted line not plotted). However, after applying a multiple linear regression to the logarithmic form of r_e , $N_{CCN,0.2\%}$ and PWV_{BL} , a significant correlation among those three variables is found. The r_e is negatively correlated with $N_{CCN,0.2\%}$ and positively correlated with PWV_{BL} , and 73.7% of the variations in binned $\ln(r_e)$ can be explained by the joint changes of the binned $\ln(N_{CCN,0.2\%})$ and $\ln(PWV_{BL})$. This indicates that in the bulk part, r_e decreases with increasing $N_{CCN,0.2\%}$ and enlarges with increasing PWV_{BL} . Notice that in the lower $N_{CCN,0.2\%}$ bins ($<150 \text{ cm}^{-3}$) where the PWV_{BL} values are the lowest among all the bins ($0.76 - 0.85 \text{ cm}$), the limitation of cloud droplet growth by competing for the available water vapor is evident by the changes in N_c and r_e . For example, the $N_{CCN,0.2\%}$ changes from 47 to 128 cm^{-3} , the N_c increases from 37 to 71 cm^{-3} and r_e only increases from 9.30 to 9.74 μm . In other words, nearly tripling the CCN loading leads to roughly doubling N_c , while the r_e is only enlarged by 0.44 μm (4.7%). In the relatively low available PWV_{BL} regime, it is clear that even with more CCN being converted into cloud droplets, the limited water vapor condition prohibits the further diffusional growth of those cloud droplets. However, in the higher $N_{CCN,0.2\%}$ bins ($>150 \text{ cm}^{-3}$) with relatively higher PWV_{BL} , the binned r_e values fluctuate and decrease with increasing CCN bins under similar PWV_{BL} (i.e., the two $N_{CCN,0.2\%}$ ranges from 200-400 cm^{-3} , and from 400-500 cm^{-3}). Since r_e essentially represents the area-weighted information of the cloud droplet size distribution (DSD), this sorting method of r_e inevitably entangles multiple cloud droplet evolution processes and environmental effects that can alter the DSD, especially under the condition of sufficient water supply. Therefore, the further assessment of the r_e responses to the $N_{CCN,0.2\%}$ loading under the constraint of water vapor should be discussed in order to untangle the impacts of different processes and environmental effects on r_e .

3.3 Aerosol-cloud interaction under different water vapor availabilities

As previously discussed above and suggested by earlier studies, the conditions of water vapor supply have a substantial impact on various processes from CCN- N_c conversion to in-cloud droplet condensational growth and coalescence processes, hence effectively altering the cloud DSD (Feingold et al., 2006; McComiskey et al., 2009; Zheng et al., 2020). Moving forward to examine how r_e responds to the changes of $N_{CCN,0.2\%}$ in the context of given water vapor availability, an index describing the aerosol-cloud interaction process is introduced as follows:

$$ACI_r = - \left. \frac{\partial \ln(r_e)}{\partial \ln(N_{CCN,0.2\%})} \right|_{PWV_{BL}}. \quad (3)$$

The ACI_r represents the relative change of r_e with respect to the relative change of $N_{CCN,0.2\%}$, where positive ACI_r denotes the decrease of r_e with increasing $N_{CCN,0.2\%}$ under binned PWV_{BL} . This

assessment of ACI_r focuses on the relative sensitivity of the cloud microphysics response in the water vapor stratified environment, while previous studies used the cloud liquid water path (LWP) as the constraint (Twomey, 1977; Feingold et al., 2003; Garrett et al., 2004). LWP describes the liquid water (i.e., existing cloud droplets) physically linked to r_e and N_c which have an interdependent relationship in cloud retrieval procedures, and hence to a certain extent, share co-variabilities with cloud microphysical properties (Dong et al., 1998; Wu et al., 2020a). In this study, by using the PWV as a sorting variable, we are trying to capture the role of ambient available water vapor in the cloud droplet growth process (especially the water vapor diffusional growth), using measurement independent to the cloud retrievals. Fig. 3 shows the variation of ACI_r under different PWV_{BL} bins, and illustrates the calculation of ACI_r in three different PWV_{BL} ranges. Note that in Fig. 3a, the regressions are derived from all points (statistically significant with a confidence level of 95%). As shown in Fig. 3a, the ACI_r values range from close-to-zero values (-0.01) to 0.22, with the mean value of 0.117 ± 0.052 . The ACI_r range of this study agrees well with the previous studies of MBL cloud aerosol-cloud interactions (McComiskey et al., 2009; Pandithurai et al., 2009; Liu et al., 2016). It is noteworthy that the variation of ACI_r with PWV_{BL} suggests two different relationships under separated PWV_{BL} conditions, as discussed in the following two paragraphs.

Under the relatively lower PWV_{BL} condition (<1.2 cm), the low values of ACI_r (-0.01 - 0.057) indicate that r_e is less sensitive to $N_{CCN,0.2\%}$, and the dependence on PWV_{BL} is also insignificant given by the flat regression line (green dashed line) and low correlation coefficient of 0.38 (Fig. 3a). As discussed in section 3.2, the limited water vapor can weaken the ability of condensational growth of the cloud droplet converted from CCN, that is, the increase of CCN loading cannot be effectively reflected by a decrease in r_e . For example, a 307% increase of $N_{CCN,0.2\%}$ only leads to a 10% decrease in r_e in the PWV_{BL} range of 0.8-1.0 cm as shown in Fig. 3b. So that in this regime, even with a slight PWV_{BL} increase, the lack of a sufficient amount of large cloud droplets is favorable to the predominant condensational growth process, which effectively narrows the cloud DSD and, in turn, confines the variable range of r_e with respect to $N_{CCN,0.2\%}$ (Pawlowska et al., 2006; Zheng et al., 2020). In this situation, the abilities of CCN to cloud droplet conversion and the droplet condensational growth are limited by insufficient water vapor, rather than an influx of CCN.

However, under the relatively higher PWV_{BL} regime (>1.2 cm), the ACI_r values become more positive and express a significant increasing trend with PWV_{BL} (correlation coefficient of 0.83, blue dashed line), which indicates that r_e is more susceptible to $N_{CCN,0.2\%}$ in this regime. On the one hand, due to the sufficient water vapor supply, the enhanced condensational growth process allows more CCN

to grow into cloud droplets, so that the limiting factor of the droplet growth corresponds to the changes in CCN loading. On the other hand, the increased N_c values associated with higher water vapor supply in the cloud effectively enhance the coalescence process. This results in broadening the cloud DSD and increasing the variation range of r_e in response to the changes of $N_{CCN,0.2\%}$. To test our hypothesis of active coalescence under higher water vapor conditions, Table 2 lists the occurrence frequencies of large r_e values (> 12 and $14 \mu\text{m}$) under the six high PWV_{BL} bins ($1.2 - 2.4 \text{ cm}$), because this range of $12-14 \mu\text{m}$ can serve as the critical demarcation of an efficient coalescence process (Gerber, 1996; Freud and Rosenfeld, 2012; Rosenfeld et al., 2012). As listed in Table 2, for the six high PWV_{BL} bins, the occurrence frequencies of $r_e > 12 \mu\text{m}$ are 25.0%, 30.6%, 54.1%, 74.2%, 93.8% and 97.5%, and the occurrence frequencies of $r_e > 14 \mu\text{m}$ are 1.25%, 1.77%, 7.4%, 17.7%, 31.9% and 20.1%, respectively.

The increasing trends of large r_e occurrences mimic the trend of ACI_r and suggest that with increased PWV_{BL}, cloud droplets have a greater chance to grow via the effective coalescence process and subsequently lead to an enlargement of ACI_r . Although previous studies have brought up the potential impacts of the cloud droplet coalescence process on ACI , it is rarely seen that the relationship among them has been discussed in detail. Here we provide possible explanations on how the enhanced coalescence process can enlarge ACI_r . Quantitatively, ACI_r is described by the log partial derivative ratio of r_e to $N_{CCN,0.2\%}$, thus a sharper decrease of r_e with respect to a given $N_{CCN,0.2\%}$ range can result in a steeper slope and in turn, larger ACI_r (i.e., a 239% increase in $N_{CCN,0.2\%}$ leads to a r_e decrease of 48% in the 2.2-2.4 cm bin in Fig. 3b). Physically, this relies on how the cloud droplet size distribution (DSD) would change with different CCN loadings. Therefore, particularly in low CCN conditions, sufficient water vapor availability will allow cloud droplets to continuously grow via diffusion of water vapor (i.e., condensational growth), and enter the active cloud-droplet coalescence regime. In contrast, the increase in cloud droplet size can effectively reduce N_c via the process of large cloud droplets collecting small droplets, and small droplets be coalesced into large droplets. Consequently, the cloud DSD becomes effectively broadened toward the large tail by the coalescence, so that r_e is enlarged. With more CCN available, the cloud DSD is narrowed by the enhanced condensational growth and regresses toward the small tail by increasing the amount of newly converted cloud droplets which result in decreased r_e . These interactions between CCNs and cloud droplets ultimately result in the broadened changeable range of r_e , and in turn, the enlarged ACI_r .

In order to investigate the theoretical implication of supersaturation conditions on the aerosol-cloud interaction observed here in the MBL stratiform clouds, the ACI_r values are calculated with respect to the surface N_{CCN} theoretically at two additional high supersaturation levels (0.5% and 1.2%), under all

PWV_{BL} conditions. The results in Table 3 show that the ACI_r signals are both weak and do not have significant changes under relatively lower PWV_{BL} conditions, while the ACI_r signals tend to strengthen with the increase of supersaturation under the relatively higher PWV_{BL}. Base on the Köhler theory, if the supersaturation exceeds the critical point for the given droplet, the droplet will thus experience continued growth, so theoretically the ACI should increase with the supersaturation under same aerosol number concentration. However, the observed limited water vapor cannot support this ideal droplet growth, results in weak responses of cloud droplets to aerosol intrusion. With the increase of observed water vapor, the continued growth of cloud droplets becomes more plausible, hence the high supersaturation yields larger droplets with low number of aerosols, more efficient droplet activation with a large number of aerosols, and in turns, larger ACI_r (even out of the theoretical bounds). However, considering these high supersaturation environments are unphysical in the observed MBL cloud layers, and estimating the real supersaturation conditions using ground-based remote-sensing is beyond the scope of this study, we chose the supersaturation level of 0.2% because it represents the most typical supersaturation conditions of MBL stratiform clouds.

3.4 The co-variabilities of the meteorological factors

The environmental conditions over the ENA have been widely studied as not independent but entangled with each other (Wood et al., 2015; Zheng et al., 2016; Wu et al., 2017; Wang et al., 2021). To better understand the dependencies and the co-variabilities of the meteorological factors, a principal component analysis (PCA) is performed targeting on the following variables: (1) PWV_{BL} denotes the water vapor availabilities within the boundary layer; (2) D_i describes the boundary layer coupling conditions; (3) TKE_w represents the strength of boundary layer turbulence; (4) $W_{dir,NS}$ reflects the surface wind directions in terms of northerly and southerly; and (5) LTS infers the large-scale thermodynamic structures. Note that the $W_{dir,NS}$ are taken as $W_{dir,NS} = abs(W_{dir} - 180^\circ)$, so that the original W_{dir} (0-360°) can be transformed to $W_{dir,NS}$ (0-180°) where the values smaller than 90° are close to the southerly wind, and those greater than 90° are close to the northerly wind. The $W_{dir,ns}$ are transformed as such to capture the island effects better, because the cliff is located north of the ENA site.

The input data metric is constructed from the above five variables to apply the PCA, and the principal components (PCs) that serving to explain the variation of those dependent variables can be output from the eigenanalysis. The result shows that for the five selected meteorological factors, the proportions of the total intervariable variance explained by the PCs are 43.72%, 22.01%, 18.26%, 8.95% and 7.06%, and the eigenvalues are 2.19, 1.10, 0.91, 0.45, and 0.35, respectively. Note that the first three

908 PCs have the highest eigenvalues and explain most (~84%) of the total variance, which indicates that
909 they can capture the significant variation patterns of the selective meteorological factors.

910 To determine the relative contributions of the variables to PCs, all the five selected meteorological
911 variables are projected to the first three PCs and the Pearson correlation coefficients between them are
912 listed in Table 4. For the first PC (PC1) which accounts for the highest proportion (43.72%) of the total
913 variance, the PC1 is strongly negatively correlated with PWV_{BL} (-0.84) and D_i (-0.73), but strongly
914 positively correlated with TKE_w (0.69). These results suggest that PC1 mainly represents the boundary
915 layer conditions, and the co-variations of the boundary layer water vapor and turbulence are the most
916 distinct environmental patterns for the selected cloud cases. The PC2 and PC3 are most correlated with
917 LTS (0.58 and 0.65 for PC2 and PC3, respectively) and $W_{dir,NS}$ (0.60 and -0.50 for PC2 and PC3,
918 respectively), indicating that the PC2 and PC3 mainly describe the variations in large-scale
919 thermodynamic and the surface wind patterns, which are likely associated with the variations of the
920 Azores High position and strength (Wood et al., 2015).

921 To further understand the correlations between the meteorological variables, the principal
922 component loadings plot is constructed by projecting the variables onto PC1 and PC2 as shown in Fig.
923 4. Each point denotes the variable correlations with PC1 (x-coordinate) and PC2 (y-coordinate), so that
924 each vector represents the strength and direction of the original variable influences on the pair of PCs.
925 The angle between the two vectors represents the correlation between each other. In Fig. 4, both TKE_w
926 and $W_{dir,NS}$ vectors are located in the same quadrant (positive in both PC1 and PC2) and close to each
927 other with a small degree of an acute angle, which means the TKE_w are strongly correlated with the
928 $W_{dir,NS}$. When the surface wind is coming from the north side of the island, the topographic lifting effect
929 of the cliff would induce additional updraft over the ENA site (Zheng et al., 2016), so that the wind closer
930 to the northerly wind (larger $W_{dir,NS}$) is more correlated with higher TKE_w . Note that TKE_w and D_i
931 vectors are almost in an opposite direction, which denotes a strongly negative correlation between the
932 two variables. The angles of PWV_{BL} with D_i (~45°) and TKE_w (~142°) suggest that PWV_{BL} is
933 moderately positively correlated with D_i but negatively correlated with TKE_w . A higher D_i indicates a
934 more decoupled MBL, where MBL is not well-mixed and separated into a radiative-driven layer and a
935 surface flux driven layer that caps the surface moisture (Jones et al., 2011). This situation is more likely
936 to associate with a relatively higher PWV_{BL} and weaker TKE_w condition. As for the LTS parameter, the
937 close to 90° angle with TKE_w suggests no correlation between them, since the LTS is mostly capturing
938 the large-scale thermodynamical structures and is obtained from a coarser temporal resolution. Thus, the
939 LTS does not essentially have correspondence to the strength of boundary layer turbulence and can be

940 treated as independent to TKE_w over the ENA site. The loading plot intuitively tells us the directions and
 941 strengths of the co-variabilities of the selected meteorological variables, and sheds the light on
 942 determining the key factors that are feasible to use in examining the environmental impacts on the
 943 aerosol-cloud interactions.

945 **3.5 Linking the meteorological factors to aerosol-cloud interaction**

947 **3.5.1 Relations of meteorological factors with aerosol and cloud properties**

948 The PCs are, mathematically, the linear combination of the selected variables, and hence
 949 independent of each other after the PCA. Therefore, treating the aerosol and cloud properties as
 950 dependents and correlated with the PCs allows us to infer their co-variation with the meteorological
 951 factors statistically. A weakly negative correlation between $N_{CCN,0.2\%}$ and PC1 ($R_{PC1,CCN} = -0.35$)
 952 suggests that the relatively higher $N_{CCN,0.2\%}$ could be sometimes found under higher PWV_{BL} and lower
 953 TKE_w . Though the correlation is low, the plausible contributions could come from the seasonal variations
 954 of $N_{CCN,0.2\%}$ and PWV_{BL} as discussed in the previous section, and the weaker TKE_w might prevent the
 955 vertical mixing of CCN and induce higher surface $N_{CCN,0.2\%}$. On the other hand, a weakly positive
 956 correlation between $N_{CCN,0.2\%}$ and PC2 ($R_{PC2,CCN} = 0.21$) suggests that there are no fundamental
 957 relationships between CCN with thermodynamic and the surface wind direction, and they are not the key
 958 controlling factor of surface $N_{CCN,0.2\%}$ variation because the surface CCN concentration is primarily
 959 contributed by the accumulation-mode aerosols which come from the condensational growth of Aitken-
 960 mode aerosols (Zheng et al., 2018). As for the cloud properties, both N_c and f_{ad} are negatively correlated
 961 with PC1 ($R_{PC1,N_c} = -0.51$ and $R_{PC1,f_{ad}} = -0.62$, respectively), suggesting a moderate relationship
 962 between N_c , f_{ad} , and the boundary layer condition. Moreover, their low correlations with PC2
 963 ($R_{PC2,N_c} = -0.10$ and $R_{PC2,f_{ad}} = -0.17$, respectively) indicate very weak relations with the large-scale
 964 thermodynamic variables. Note that the same sign of correlations with PC1 statistically inferring the
 965 similar directional co-variation of $N_{CCN,0.2\%}$, N_c , and f_{ad} to a certain extent.

966 To examine the physical relation between $N_{CCN,0.2\%}$, N_c and f_{ad} , the profiles of cloud r_e and
 967 LWC are plotted in normalized height from cloud base (z_b) to cloud top height (z_t) (Fig. 5), which is
 968 given by $z_n = (z - z_b) / (z_t - z_b)$. The solid lines denote the mean values, and the shaded area
 969 represents one standard deviation at each normalized height z_n . The normalized r_e increases from ~ 8.6
 970 μm at the cloud base toward $\sim 11 \mu m$ near the upper part of the cloud where z_n is 0.7 (Fig. 5a), through
 971 condensational growth and coalescence processes, and then decreases toward the cloud top due to cloud-

top entrainment. Similar in-cloud vertical variation of r_e is also found by previous study using aircraft in-situ measurements (Zhao et al., 2018; Wu et al. 2020a). Profiles of retrieved LWC and calculated adiabatic LWC_{ad} (blue line) are presented in Fig. 5b. As demonstrated in Fig. 5b, the f_{ad} values, which is the ratio of LWC to LWC_{ad}, reach a maximum of 0.8 at the cloud base and a minimum of 0.38 at the cloud top. The shaded areas of r_e and LWC denote the range from near-adiabatic to sub-adiabatic cloud environments, where in the near-adiabatic cloud (higher f_{ad}) the cloud droplets experience adiabatic growth and LWC should close to LWC_{ad}. In contrast, in the sub-adiabatic cloud regime, the decrease of f_{ad} is largely due to cloud-top entrainment and coalescence processes even in non-precipitating MBL clouds (Wood, 2012; Braun et al., 2018; Wu et al. 2020b). Furthermore, to understand the implication of cloud adiabaticity with respect to CCN- N_c conversion, all of the f_{ad} samples are separated into two groups by the median value of the layer-mean f_{ad} (0.66) for a further analysis.

Figure 6 shows N_c against the binned $N_{CCN,0.2\%}$ for the near-adiabatic regime ($f_{ad} > 0.66$) and sub-adiabatic regime ($f_{ad} < 0.66$). For the near-adiabatic regime, N_c increases from $\sim 60 \text{ cm}^{-3}$ to 119 cm^{-3} with increased $N_{CCN,0.2\%}$ and PWV_{BL}, and both $N_{CCN,0.2\%}$ and PWV_{BL} appear to play positive roles in terms of the N_c increase. The result is as expected because the process of condensational growth is predominant in the near-adiabatic clouds, that is, with increasing water vapor supply, the higher CCN loading can effectively lead to more cloud droplets. However, in the sub-adiabatic cloud regime, N_c increases with increased $N_{CCN,0.2\%}$ but possesses a negative correlation with PWV, which results in a slower increase of N_c under higher $N_{CCN,0.2\%}$ and PWV_{BL} conditions. The mean reduction of N_c in the sub-adiabatic regime is computed to be $\sim 37\%$ compared to that for the near-adiabatic clouds. As previously studied, the coalescence process contributes significantly to N_c depletion, even in a non-precipitating MBL clouds (Feingold et al., 1996; Wood, 2006). Thus, lower N_c in the sub-adiabatic regime may be partly due to the combined effect of coalescence and entrainment (Wood, 2006; Hill et al., 2009; Yum et al., 2015; Wang et al., 2020). Note that the retrieved N_c is representing the cloud layer-mean information. In summary, the Wu et al. (2020a) retrieval works as separating the reflectivity to the contributions of cloud (Z_c) and drizzle, the cloud procedure assumes an initial guess of the representative layer-mean N_c based on the climatology over ENA sites (Dong et al., 2014), and such allows the first guess of the vertical profile of LWC based on N_c and Z_c , and then constrains back the N_c and LWC using the LWP from MWR, finally output r_e (Fig.3 in Wu et al., 2020a). Therefore, the final retrieved N_c is updated to in response to the cloud microphysical processes within this time-step. From the aircraft in-situ measurements during the ACE-ENA, we used the in-situ measurement during ACE-ENA to validate the retrieval outputs and found that the observed N_c profile is near-constant in middle part of the cloud,

with the signal of entrainment-induced depletion near the cloud top, even in the drizzling cloud where the collision-coalescence processes are more active (Wu et al., 2020a). However, it is hard and beyond the scope of the ground-based retrieval to compare the vertical dependency of depletion rate within one time-step. Therefore, as the retrieval currently work as representing the layer-mean information from the given time-step, the preferred method in this study is to compare N_c at different times, where in this case are the adiabatic versus sub-adiabatic conditions which hence yields different N_c that we retrieved from the ground-based snapshot perspective. From the PCA and binning analysis, the effect of cloud adiabaticities on CCN- N_c conversions may shed light on interpreting the aerosol-cloud interaction under different environmental effects.

3.5.2 The role of meteorological factors on ACI_r assessment

Since ACI_r can only be calculated by the logarithmic derivatives from a set of $N_{CCN,0.2\%}$ and r_e data within a certain regime, it will be inappropriate to linearly correlate the data with PCs directly, in both mathematical and physical perspectives. Therefore, the meteorological factors which have the strongest influence on the most explanatory PCs, namely PWV_{BL} and TKE_w are selected to be the sorting variables in assessing the environmental impacts on the ACI_r . In addition, LTS is also selected as it represents the large-scale thermodynamic factor and is independent to the boundary-layer environment conditions. The data samples are first separated into two regimes using the median values of the targeting factors, and then separated into four quadrants by the median PWV_{BL} because ACI_r is found to have significant differences under different water vapor availabilities. The ACI_r values are further calculated for all quadrants to examine whether the ACI_r can be distinguished by the targeting factors.

Combining LTS and PWV_{BL} as sorting variables, the ACI_r values for four regimes are shown in Fig. S4. The ACI_r differences between low and high PWV_{BL} regimes are still retained. In the low PWV_{BL} regime, the ACI_r values are limited to 0.016 and 0.056 for low and high LTS regimes, respectively. In the high PWV_{BL} regime, the ACI_r values are 0.150 and 0.171 for low and high LTS regimes, respectively, which is about 3-5 times greater than those in low PWV_{BL} regime. However, the ACI_r in different LTS regimes cannot be distinctly differentiated (ACI_r differences between LTS regimes are ~ 0.02 and ~ 0.04), and the main difference in ACI_r are still induced by the PWV_{BL} . Owing to the location of the ENA site where it locates near the boundary of mid-latitude and subtropical climate regimes, the MBL clouds over the ENA are found to be often under the influences of cold fronts associated with mid-latitude cyclones, where the cloud evolutions are subject to the combine effects of post-frontal and large-scale subsidence (Wood et al., 2015; Zheng et al., 2020; Wang et al., 2021). Therefore, over the ENA, although the spatial

1036 gradient of LTS is studied to be associated with the production of MBL turbulence and the change in
1037 wind direction (Wu et al., 2017), the LTS value itself is examined to have a weak impact on the aerosol-
1038 cloud interaction from this study.

1039 The TKE_w has been found to be strongly positively correlated with $W_{dir,NS}$ and negatively
1040 correlated with D_i from the PCA, that is, the values of TKE_w already account for the co-variabilities in
1041 these variables. Therefore, treating TKE_w as the sorting variable would lead to a more physical process-
1042 orientated assessment. Accordingly, to examine the role of the dynamical factors on ACI_r , the samples
1043 are separated into four regimes demarcated by the median values of PWV_{BL} and TKE_w (Fig. 7), and the
1044 mean values of D_i and f_{ad} in the four quadrants are also displayed in Fig. 7. The effect of PWV_{BL} on
1045 ACI_r is demonstrated by the mean ACI_r values where they are much higher in the high PWV_{BL} regime
1046 than those in the low PWV_{BL} regime no matter what the TKE_w regimes. Furthermore, the result illustrates
1047 that TKE_w does play an important role in ACI_r , because the ACI_r values in the high TKE_w regime are
1048 more than double than the values in the low TKE_w regime.

1049 In the regimes of high TKE_w and PWV_{BL} , which are closely associated with coupled MBL ($D_i =$
1050 0.21) and more sub-adiabatic cloud conditions ($f_{ad} = 0.52$), r_e is highly sensitive to CCN loading with
1051 the highest ACI_r of 0.259. The sufficient water vapor availability allows CCN to be converted into cloud
1052 droplets more effectively, while the relatively higher TKE_w indicates stronger turbulence in the below-
1053 cloud boundary layer and maintains a nearly well-mixed MBL. The CCN and moisture below-cloud layer
1054 are efficiently transported and mixed aloft via the ascending branch of the eddies (Nicholls, 1984; Hogan
1055 et al., 2009), hence are effectively connected to the cloud layer. Therefore, under the lower CCN loading
1056 condition, the active coalescence process (which indicated by the low f_{ad} values) results in the depletion
1057 of small cloud droplets and broadening of cloud DSD (Chandrakar et al., 2016), and in turn, leads to
1058 further enlarged r_e . However, with higher CCN intrusion into the cloud layer, the enhanced cloud droplet
1059 conversion and the subsequential condensational growth behave contradictorily to narrow the DSD
1060 (Pinsky and Khain, 2002; Pawlowska et al., 2006), which leads to decreased r_e . Therefore, the MBL
1061 clouds are distinctly susceptible to CCN loading under the environments of sufficient water vapor and
1062 strong turbulence in which the ACI_r is enlarged.

1063 Under high PWV_{BL} but low TKE_w conditions, the mean ACI_r reduces to 0.101 (~ 39% of that
1064 under high TKE_w). The MBL is more likely decoupled where $D_i = 0.54$, which indicates that the weaker
1065 turbulence loosens the connection between the cloud layer and the underlying boundary layer. This
1066 results in a less effective conversion of CCN into cloud droplets, while the more adiabatic cloud
1067 environment ($f_{ad} = 0.75$) denotes the lack of coalescence growths and thus diminishes the r_e sensitivity

to CCN. Although the constraints of insufficient water vapor on ACI_r are still evident, the ACI_r values increase from 0.008 in the low TKE_w regime to 0.024 in the high TKE_w regime. The ACI_r differences between the two TKE_w regimes attest that ACI_r strongly depends on the connection between the cloud layer and the below-cloud boundary layer CCN and moisture, that is, stronger turbulence can enhance the susceptibility of r_e to CCN.

In this study, the relationship between turbulence and ACI is found to be valid in non-precipitating MBL clouds. Theoretically, the effect of turbulence on ACI_r would appear to be artificially amplified, if in the presence of precipitation. The intensive turbulence can enhance the coalescence process and accelerate the CCN-cloud cycling, and subsequently, the CCN depletion due to precipitation and coalescence scavenging would result in quantitatively enlarged ACI_r (Feingold et al., 1996, 1999; Duong et al., 2011; Braun et al., 2018). Though it is beyond the scope of this study, it would be of interest to perform such analysis on the aerosol-cloud-precipitation interaction using ground-based remote sensing and model simulations in the future study.

4. Summaries and Conclusions

Over the ARM-ENA site, a total of 20 non-precipitating single-layered MBL stratus and stratocumulus cloud cases have been selected in order to investigate the aerosol-cloud interaction (ACI). The distributions of CCN and cloud properties for selected cases represent the typical characteristics of non-precipitating MBL clouds in a relatively clean environment over the remote oceanic area. The diversity of boundary layer conditions and cloud adiabaticities among the selected cases enable the investigation of different environmental effects on ACI.

The overall variations of N_c with $N_{CCN,0.2\%}$ show an increasing trend, regardless of the water vapor condition, while the sufficient PWV_{BL} appears to stabilize the CCN- N_c conversion process. The water vapor limitation on cloud droplet growth is evident in the lower $N_{CCN,0.2\%}$ up to 150 cm^{-3} with low PWV_{BL} values, where a near tripling of CCN loading leads to a near doubling of N_c but only 4.7% increase in r_e . When $N_{CCN,0.2\%}$ is greater than 250 cm^{-3} and PWV_{BL} values are also relatively high, r_e appears to decrease with increasing $N_{CCN,0.2\%}$ under similar water vapor conditions. As for bulk aerosol-cloud interaction, the ACI_r values vary from -0.01 to 0.22 for different PWV_{BL} conditions where ACI_r appears to be diminished under limited water vapor availability due to the limited droplet activation and condensational growth process. While under relatively sufficient water supply condition, r_e shows more sensitive responses to the changes of $N_{CCN,0.2\%}$, due to the combined effect of condensational growth and coalescence processes accompanying the higher N_c and PWV_{BL} .

1100 The theoretical diagram describing the mechanism proposed above is shown in Fig. 8. Under the
 1101 relatively lower PWV_{BL} condition, the limited water vapor weakens the ability of condensational growth
 1102 of the cloud droplet converted from CCN, which results in both less newly converted as well as large
 1103 cloud droplets, with the lack of chance of coalescence process under this circumstance. Therefore, the
 1104 variable range of r_e versus $N_{CCN,0.2\%}$ is narrowed and presented as small ACI_r . While under the relatively
 1105 higher PWV_{BL} condition, particularly in low CCN conditions, the sufficient water vapor availability
 1106 allows cloud droplets growing via the condensation of water vapor, and thus enter the active cloud-
 1107 droplet coalescence regime. In contrast, the increase in cloud droplet size can effectively reduce N_c via
 1108 the coalescence process and the size distributions are effectively broadened toward the large tail by the
 1109 coalescence, so that r_e is enlarged. Under a higher $N_{CCN,0.2\%}$ intrusion, the cloud droplet size distribution
 1110 is narrowed by the enhanced condensational growth and regresses toward the small tail by increasing the
 1111 amount of newly converted cloud droplets which results in decreased r_e . Combinedly, the interactions
 1112 between CCNs and cloud droplet growing processes ultimately result in a broadened changeable range
 1113 of r_e , and in turn, the enlarged ACI_r .

1114 The co-variabilities among the environmental factors are examined using the multi-dimensional
 1115 PCA. The variables of PWV_{BL} , D_i , TKE_w , LTS and $W_{dir,NS}$ are constructed as the input of the
 1116 eigenanalysis. Results show that the first three PCs can describe the majority (~84%) of the variance
 1117 among the selected variables. The most explanatory PC1 (account for 43.72% contribution) strongly
 1118 correlated with PWV_{BL} , D_i (both negatively) and TKE_w (positively), and hence describe the co-variation
 1119 of the boundary layer conditions. While the PC2 and PC3 (account for 22.01% and 18.26% contributions,
 1120 respectively) are strongly correlated with LTS and $W_{dir,NS}$, which likely indicates the variations of the
 1121 Azores High position and strength. By projecting the variables onto PC1 and PC2, the PCA loading
 1122 analysis shows that TKE_w is strongly negatively correlated with D_i , which is what we expected. A
 1123 decoupled MBL cloud is often separated into two layers where the lower one can cap the surface moisture,
 1124 while the higher TKE_w denote sufficient turbulence that maintains the well-mixed MBL. Additionally,
 1125 the island effect is also indicated by the eigenanalysis, where surface northerly wind would induce
 1126 additional updraft velocity and hence disturb TKE_w , owing to the topographic effect of the cliff north of
 1127 the ENA site. The role of cloud adiabaticities on the behaviors of CCN- N_c conversion is examined using
 1128 both binning and eigenanalysis. In a near-adiabatic cloud vertical structure, the cloud droplet growing
 1129 process is dominated by condensational growth, thus the N_c responses to increased $N_{CCN,0.2\%}$ and
 1130 PWV_{BL} are strengthened. When the cloud layer becomes more sub-adiabatic, the effect of coalescence
 1131 leads to the depletion of N_c and thus results in the lower retrieved N_c from a ground-based snapshot

perspective. The competition between the condensational growth and coalescence processes strongly impacts the variations of cloud microphysics to CCN loading.

To investigate the environmental effects on ACI_r , the factors having the most influence on the explanatory PCs are selected as the sorting variables in the ACI_r assessments. The LTS sorting method cannot distinguish the ACI_r values, which means the LTS values themselves have a weak impact on ACI_r due to the MBL cloud cover over the ENA is mainly impacted by the mid-latitude cyclone systems. In contrast, the intensity of boundary layer turbulence represented by TKE_w plays a more important role in ACI_r , since the values of TKE_w already account for the co-variations of the MBL conditions, and hence leads to a physical process-orientated assessment. The ACI_r assessments in four different TKE_w and PWV_{BL} regimes show that the constraints of insufficient water vapor on the ACI_r are still evident, but in both PWV_{BL} regimes the ACI_r values increase more than double from low TKE_w to high TKE_w regimes. Noticeably, the ACI_r increases from 0.101 in the low TKE_w regime to 0.259 in the high TKE_w regime, under high PWV_{BL} conditions. The intensive below-cloud boundary layer turbulence strengthens the connection between the cloud layer and below-cloud CCN and moisture. So that with sufficient water vapor, an active coalescence leads to further enlarged r_e , particularly for low CCN loading condition, while the enhanced N_c from condensational growth induced by increased $N_{CCN,0.2\%}$ can effectively decrease r_e . Combining these processes together, the enlarged ACI_r is presented.

In this study, the non-precipitating MBL clouds are found to be most susceptible to the below-cloud CCN loading under environments with sufficient water vapor and stronger turbulence. This study examines the importance of the environmental effects on the ACI_r assessments, and provides the observational constraints to the future model evaluations on the aerosol-cloud interactions. Future studies will be focusing on exploring the role of environmental effects on the aerosol-cloud-precipitation interactions in MBL stratocumulus through an integrative analysis of observations and model simulations.

1155
1156

Data availability. Data used in this study can be accessed from the DOE ARM's Data Discovery at <https://adc.arm.gov/discovery/>

1159

Author contributions. The original idea of this study is discussed by XZ, BX, and XD. XZ performed the analyses and wrote the manuscript. XZ, BX, XD, PW, YW and TL participated in further scientific discussions and provided substantial comments and edits on the paper.

1163

Competing interests. The authors declare that they have no conflict of interest.

1164

1165

1166 *Special issue statement.* This article is part of the special issue “Marine aerosols, trace gases, and clouds
1167 over the North Atlantic (ACP/AMT inter-journal SI)”. It is not associated with a conference.

1168

1169 *Acknowledgments.* The ground-based measurements were obtained from the Atmospheric Radiation
1170 Measurement (ARM) Program sponsored by the U.S. Department of Energy (DOE) Office of Energy
1171 Research, Office of Health and Environmental Research, and Environmental Sciences Division. The
1172 reanalysis data were obtained from the ECMWF model output, which provides explicitly for the analysis
1173 at the ARM ENA site. The data can be downloaded from <https://adc.arm.gov/discovery/>. This work was
1174 supported by the NSF grants AGS-1700728/1700727 and AGS-2031750/2031751, and was also
1175 supported as part of the “Enabling Aerosol-cloud interactions at GLobal convection-permitting scales
1176 (EAGLES)” project (74358), funded by the U.S. Department of Energy, Office of Science, Office of
1177 Biological and Environmental Research, Earth System Modeling program with the subcontract to the
1178 University of Arizona. The Pacific Northwest National Laboratory is operated for the Department of
1179 Energy by Battelle Memorial Institute under Contract DE-AC05-76 RL01830. And a special thanks to
1180 three anonymous reviewers for the constructive comments and suggestions, which helped to improve the
1181 manuscript.

1182

1183 **References.**

1184 Albrecht, B. A., Bretherton, C. S., Johnson, D., Schubert, W. H. and Frisch, A. S.: The Atlantic
1185 Stratocumulus Transition Experiment - ASTEX, Bull. - Am. Meteorol. Soc., doi:10.1175/1520-
1186 0477(1995)076<0889:TASTE>2.0.CO;2, 1995.

1187 ARM MET Handbook: ARM Surface Meteorology Systems (MET) Handbook, DOE ARM Climate
1188 Research Facility, DOE/SC-ARM/TR-086. Available at:
1189 https://www.arm.gov/publications/tech_reports/handbooks/met_handbook.pdf, last access: 21
1190 August 2021.

1191 Braun, R. A., Dadashazar, H., MacDonald, A. B., Crosbie, E., Jonsson, H. H., Woods, R. K., Flagan, R.
1192 C., Seinfeld, J. H. and Sorooshian, A.: Cloud Adiabaticity and Its Relationship to Marine
1193 Stratocumulus Characteristics Over the Northeast Pacific Ocean, J. Geophys. Res. Atmos.,
1194 doi:10.1029/2018JD029287, 2018.

1195 Cadeddu, M. P., Liljegren, J. C. and Turner, D. D.: The atmospheric radiation measurement (ARM)
 1196 program network of microwave radiometers: Instrumentation, data, and retrievals, *Atmos. Meas.*
 1197 *Tech.*, doi:10.5194/amt-6-2359-2013, 2013.

1198 Chandrakar, K. K., Cantrell, W., Chang, K., Ciochetto, D., Niedermeier, D., Ovchinnikov, M., Shaw, R.
 1199 A. and Yang, F.: Aerosol indirect effect from turbulence-induced broadening of cloud-droplet size
 1200 distributions, *Proc. Natl. Acad. Sci. U. S. A.*, doi:10.1073/pnas.1612686113, 2016.

1201 Chen, Y. C., Christensen, M. W., Stephens, G. L. and Seinfeld, J. H.: Satellite-based estimate of global
 1202 aerosol-cloud radiative forcing by marine warm clouds, *Nat. Geosci.*, doi:10.1038/ngeo2214, 2014.

1203 Costantino, L. and Bréon, F. M.: Analysis of aerosol-cloud interaction from multi-sensor satellite
 1204 observations, *Geophys. Res. Lett.*, doi:10.1029/2009GL041828, 2010.

1205 Diamond, M. S., Dobracki, A., Freitag, S., Griswold, J. D. S., Heikkila, A., Howell, S. G., Kacarab, M.
 1206 E., Podolske, J. R., Saide, P. E. and Wood, R.: Time-dependent entrainment of smoke presents an
 1207 observational challenge for assessing aerosol-cloud interactions over the southeast Atlantic Ocean,
 1208 *Atmos. Chem. Phys.*, doi:10.5194/acp-18-14623-2018, 2018.

1209 Dong, X., Xi, B., Kennedy, A., Minnis, P. and Wood, R.: A 19-month record of marine aerosol-cloud-
 1210 radiation properties derived from DOE ARM mobile facility deployment at the Azores. Part I: Cloud
 1211 fraction and single-layered MBL cloud properties, *J. Clim.*, doi:10.1175/JCLI-D-13-00553.1, 2014.

1212 Dong, X., Schwantes, A. C., Xi, B. and Wu, P.: Investigation of the marine boundary layer cloud and
 1213 CCN properties under coupled and decoupled conditions over the azores, *J. Geophys. Res.*,
 1214 doi:10.1002/2014JD022939, 2015.

1215 Duong, H. T., Sorooshian, A. and Feingold, G.: Investigating potential biases in observed and modeled
 1216 metrics of aerosol-cloud-precipitation interactions, *Atmos. Chem. Phys.*, doi:10.5194/acp-11-4027-
 1217 2011, 2011.

1218 Fan, J., Wang, Y., Rosenfeld, D., Liu, X.: Review of Aerosol-Cloud Interactions: Mechanisms,
 1219 Significance and Challenges, *J. Atmo. Sci.* 73(11), 4221-4252, 2016.

1220 Feingold, G., Kreidenweis, S. M., Stevens, B. and Cotton, W. R.: Numerical simulations of stratocumulus
 1221 processing of cloud condensation nuclei through collision-coalescence, *J. Geophys. Res. Atmos.*,
 1222 doi:10.1029/96jd01552, 1996.

1223 Feingold, G., Frisch, A. S., Stevens, B. and Cotton, W. R.: On the relationship among cloud turbulence,
 1224 droplet formation and drizzle as viewed by Doppler radar, microwave radiometer and lidar, *J.*
 1225 *Geophys. Res. Atmos.*, doi:10.1029/1999JD900482, 1999.

1226 Feingold, G., Furrer, R., Pilewskie, P., Remer, L. A., Min, Q. and Jonsson, H.: Aerosol indirect effect
 1227 studies at Southern Great Plains during the May 2003 Intensive Operations Period, *J. Geophys. Res.*
 1228 *Atmos.*, doi:10.1029/2004JD005648, 2006.

1229 Feingold, G. and McComiskey, A.: ARM's Aerosol–Cloud–Precipitation Research (Aerosol Indirect
 1230 Effects), *Meteorol. Monogr.*, doi:10.1175/amsmonographs-d-15-0022.1, 2016.

1231 Freud, E. and Rosenfeld, D.: Linear relation between convective cloud drop number concentration and
 1232 depth for rain initiation, *J. Geophys. Res. Atmos.*, doi:10.1029/2011JD016457, 2012.

1233 Garrett, T. J. and Zhao, C.: Increased Arctic cloud longwave emissivity associated with pollution from
 1234 mid-latitudes, *Nature*, doi:10.1038/nature04636, 2006.

1235 Garrett, T. J., Zhao, C., Dong, X., Mace, G. G. and Hobbs, P. V.: Effects of varying aerosol regimes on
 1236 low-level Arctic stratus, *Geophys. Res. Lett.*, doi:10.1029/2004GL019928, 2004.

1237 Gerber, H.: Microphysics of marine stratocumulus clouds with two drizzle modes, *J. Atmos. Sci.*,
 1238 doi:10.1175/1520-0469(1996)053<1649:MOMSCW>2.0.CO;2, 1996.

1239 Ghate, V. P., Albrecht, B. A. and Kollias, P.: Vertical velocity structure of nonprecipitating continental
 1240 boundary layer stratocumulus clouds, *J. Geophys. Res. Atmos.*, doi:10.1029/2009JD013091, 2010.

1241 Ghate, V. P. and Cadeddu, M. P.: Drizzle and Turbulence Below Closed Cellular Marine Stratocumulus
 1242 Clouds, *J. Geophys. Res. Atmos.*, doi:10.1029/2018JD030141, 2019.

1243 Gryspeerd, E., Quaas, J. and Bellouin, N.: Constraining the aerosol influence on cloud fraction, *J.*
 1244 *Geophys. Res.*, doi:10.1002/2015JD023744, 2016.

1245 Hill, A. A., Feingold, G. and Jiang, H.: The influence of entrainment and mixing assumption on aerosol–
 1246 cloud interactions in marine stratocumulus, *J. Atmos. Sci.*, doi: 10.1175/2008JAS2909.1, 2009.

1247 Hogan, R. J., Grant, A. L. M., Illingworth, A. J., Pearson, G. N. and O’Connor, E. J.: Vertical velocity
 1248 variance and skewness in clear and cloud-topped boundary layers as revealed by Doppler lidar, *Q.*
 1249 *J. R. Meteorol. Soc.*, doi:10.1002/qj.413, 2009.

1250 Hudson, J. G. and Noble, S.: CCN and Vertical Velocity Influences on Droplet Concentrations and
 1251 Supersaturations in Clean and Polluted Stratus Clouds, *J. Atmos. Sci.*, doi:10.1175/jas-d-13-086.1,
 1252 2013.

1253 Jones, C. R., Bretherton, C. S., and Leon, D.: Coupled vs. decoupled boundary layers in VOCALS-REx,
 1254 *Atmos. Chem. Phys.*, 11, 7143–7153, <https://doi.org/10.5194/acp-11-7143-2011>, 2011.

1255 Klein, S. A. and Hartmann, D. L.: The seasonal cycle of low stratiform clouds, *J. Clim.*,
 1256 doi:10.1175/1520-0442(1993)006<1587:TSCOLS>2.0.CO;2, 1993.

1257 Kim, B. G., Miller, M. A., Schwartz, S. E., Liu, Y. and Min, Q.: The role of adiabaticity in the aerosol
 1258 first indirect effect, *J. Geophys. Res. Atmos.*, doi:10.1029/2007JD008961, 2008.

1259 Liu, J., Li, Z. and Cribb, M.: Response of marine boundary layer cloud properties to aerosol perturbations
 1260 associated with meteorological conditions from the 19-month AMF-Azores campaign, *J. Atmos.*
 1261 *Sci.*, doi:10.1175/JAS-D-15-0364.1, 2016.

1262 Lappen, C. L. and Randall, D. A.: Toward a unified parameterization of the boundary layer and moist
 1263 convection. Part I: A new type of mass-flux model, *J. Atmos. Sci.*, doi:10.1175/1520-
 1264 0469(2001)058<2021:TAUPOT>2.0.CO;2, 2001.

1265 Logan, T., Xi, B. and Dong, X.: Aerosol properties and their influences on marine boundary layer cloud
 1266 condensation nuclei at the ARM mobile facility over the Azores, *J. Geophys. Res.*,
 1267 doi:10.1002/2013JD021288, 2014.

1268 Logan, T., Dong, X. and Xi, B.: Aerosol properties and their impacts on surface CCN at the ARM
 1269 Southern Great Plains site during the 2011 Midlatitude Continental Convective Clouds Experiment,
 1270 Adv. Atmos. Sci., doi:10.1007/s00376-017-7033-2, 2018.

1271 Lu, M. L., Conant, W. C., Jonsson, H. H., Varutbangkul, V., Flagan, R. C. and Seinfeld, J. H.: The marine
 1272 stratus/stratocumulus experiment (MASE): Aerosol-cloud relationships in marine stratocumulus, J.
 1273 Geophys. Res., doi:10.1029/2006JD007985, 2007.

1274 Mann, J. A., Christine Chiu, J., Hogan, R. J., O'Connor, E. J., L'Ecuyer, T. S., Stein, T. H. and Jefferson,
 1275 A.: Aerosol impacts on drizzle properties in warm clouds from ARM Mobile Facility maritime and
 1276 continental deployments, J. Geophys. Res., doi:10.1002/2013JD021339, 2014.

1277 Martin, G. M., Johnson, D. W. and Spice, A.: The Measurement and Parameterization of Effective Radius
 1278 of Droplets in Warm Stratocumulus Clouds, J. Atmos. Sci., doi:10.1175/1520-
 1279 0469(1994)051<1823:tmapoe>2.0.co;2, 1994.

1280 Martins, J. V., Marshak, A., Remer, L. A., Rosenfeld, D., Kaufman, Y. J., Fernandez-Borda, R., Koren,
 1281 I., Correia, A. L., Zubko, V. and Artaxo, P.: Remote sensing the vertical profile of cloud droplet
 1282 effective radius, thermodynamic phase, and temperature, Atmos. Chem. Phys., doi:10.5194/acp-11-
 1283 9485-2011, 2011.

1284 McComiskey, A., Feingold, G., Frisch, A. S., Turner, D. D., Miller, M., Chiu, J. C., Min, Q. and Ogren,
 1285 J.: An assessment of aerosol-cloud interactions in marine stratus clouds based on surface remote
 1286 sensing, J. Geophys. Res., 114, D09203, doi:10.1029/2008JD011006, 2009.

1287 McComiskey, A. and Feingold, G.: The scale problem in quantifying aerosol indirect effects, Atmos.
 1288 Chem. Phys., doi:10.5194/acp-12-1031-2012, 2012.

1289 Medeiros, B. and Stevens, B.: Revealing differences in GCM representations of low clouds, Clim. Dyn.,
 1290 doi:10.1007/s00382-009-0694-5, 2011.

1291 Morris, V. R.: Ceilometer Instrument Handbook, DOE ARM Climate Research Facility, DOE/SC-ARM-
 1292 TR-020, 2016. Available at:

1293 https://www.arm.gov/publications/tech_reports/handbooks/ceil_handbook.pdf, last access: 23
 1294 April 2021.

1295 Newsom, R. K., Sivaraman, C., Shippert, T.R. and Riihimaki, L. D.: Doppler Lidar Vertical Velocity
 1296 Statistics Value-Added Product. DOE ARM Climate Research Facility, DOE/SC-ARM/TR-149,
 1297 2019. Available at: https://www.arm.gov/publications/tech_reports/doe-sc-arm-tr-149.pdf, last
 1298 access: 2 September 2021.

1299 Nicholls, S.: The dynamics of stratocumulus: Aircraft observations and comparisons with a mixed layer
 1300 model, Q. J. R. Meteorol. Soc., doi:10.1002/qj.49711046603, 1984.

1301 Pandithurai, G., Takamura, T., Yamaguchi, J., Miyagi, K., Takano, T., Ishizaka, Y., Dipu, S. and Shimizu,
 1302 A.: Aerosol effect on cloud droplet size as monitored from surface-based remote sensing over East
 1303 China Sea region, Geophys. Res. Lett., doi:10.1029/2009GL038451, 2009.

1304 Pawlowska, H., Grabowski, W. W. and Brenguier, J. L.: Observations of the width of cloud droplet
 1305 spectra in stratocumulus, Geophys. Res. Lett., doi:10.1029/2006GL026841, 2006.

1306 Pearson, G., Davies, F. and Collier, C.: An analysis of the performance of the UFAM pulsed Doppler
 1307 lidar for observing the boundary layer, J. Atmos. Ocean. Technol.,
 1308 doi:10.1175/2008JTECHA1128.1, 2009.

1309 Pinsky, M. B. and Khain, A. P.: Effects of in-cloud nucleation and turbulence on droplet spectrum
 1310 formation in cumulus clouds, Q. J. R. Meteorol. Soc., doi:10.1256/003590002321042072, 2002.

1311 Qiu, Y., Zhao, C., Guo, J. and Li, J.: 8-Year ground-based observational analysis about the seasonal
 1312 variation of the aerosol-cloud droplet effective radius relationship at SGP site, Atmos. Environ.,
 1313 doi:10.1016/j.atmosenv.2017.06.002, 2017.

1314 Romps, D. M.: Exact expression for the lifting condensation level, J. Atmos. Sci., doi:10.1175/JAS-D-
 1315 17-0102.1, 2017.

1316 Rosenfeld, D. and Woodley, W. L.: Closing the 50-year circle: From cloud seeding to space and back to
 1317 climate change through precipitation physics. Chapter 6 of “Cloud Systems, Hurricanes, and the

1318 Tropical Rainfall Measuring Mission (TRMM)”, edited by: Tao, W.-K. and Adler, R. F., Meteor.
1319 Monogr., 51, 234 pp., 59–80, AMS, 2003.

1320 Rosenfeld, D.: Aerosol-Cloud Interactions Control of Earth Radiation and Latent Heat Release Budgets,
1321 in *Solar Variability and Planetary Climates.*, 2007.

1322 Rosenfeld, D., Wang, H. and Rasch, P. J.: The roles of cloud drop effective radius and LWP in
1323 determining rain properties in marine stratocumulus, *Geophys. Res. Lett.*,
1324 doi:10.1029/2012GL052028, 2012.

1325 Rosenfeld, D., Zhu, Y., Wang, M., Zheng, Y., Goren, T. and Yu, S.: Aerosol-driven droplet
1326 concentrations dominate coverage and water of oceanic low-level clouds, *Science* (80-.),
1327 doi:10.1126/science.aav0566, 2019.

1328 Seinfeld, J. H., Bretherton, C., Carslaw, K. S., Coe, H., DeMott, P. J., Dunlea, E. J., Feingold, G., Ghan,
1329 S., Guenther, A. B., Kahn, R., Kraucunas, I., Kreidenweis, S. M., Molina, M. J., Nenes, A., Penner,
1330 J. E., Prather, K. A., Ramanathan, V., Ramaswamy, V., Rasch, P. J., Ravishankara, A. R., Rosenfeld,
1331 D., Stephens, G. and Wood, R.: Improving our fundamental understanding of the role of aerosol-
1332 cloud interactions in the climate system, *Proc. Natl. Acad. Sci. U. S. A.*,
1333 doi:10.1073/pnas.1514043113, 2016.

1334 Siebert, H., Szodry, K.-E., Egerer, U., Wehner, B., Henning, S., Chevalier, K., Lücknerath, J., Welz, O.,
1335 Weinhold, K., Lauermann, F., Gottschalk, M., Ehrlich, A., Wendisch, M., Fialho, P., Roberts, G.,
1336 Allwayin, N., Schum, S., Shaw, R. A., Mazzoleni, C., Mazzoleni, L., Nowak, J. L., Malinowski, S.
1337 P., Karpinska, K., Kumala, W., Czyzewska, D., Luke, E. P., Kollias, P., Wood, R. and Mellado, J.
1338 P.: Observations of Aerosol, Cloud, Turbulence, and Radiation Properties at the Top of the Marine
1339 Boundary Layer over the Eastern North Atlantic Ocean: The ACORES Campaign, *Bull. Am.*
1340 *Meteorol. Soc.*, doi:10.1175/bams-d-19-0191.1, 2021.

1341 Thorsen, T. J. and Fu, Q.: Automated retrieval of cloud and aerosol properties from the ARM Raman
1342 Lidar. Part II: Extinction, *J. Atmos. Ocean. Technol.*, doi:10.1175/JTECH-D-14-00178.1, 2015.

1343 Toto, T, and Jensen, M: Interpolated Sounding and Gridded Sounding Value-Added Products. DOE
 1344 ARM Climate Research Facility, DOE/SC-ARM-TR-183, 2016. Available at:
 1345 https://www.arm.gov/publications/tech_reports/doe-sc-arm-tr-183.pdf, last access: 2 September
 1346 2021.

1347 Twohy, C. H., Petters, M. D., Snider, J. R., Stevens, B., Tahnk, W., Wetzel, M., Russell, L. and Burnet,
 1348 F.: Evaluation of the aerosol indirect effect in marine stratocumulus clouds: Droplet number, size,
 1349 liquid water path, and radiative impact, J. Geophys. Res. D Atmos., doi:10.1029/2004JD005116,
 1350 2005.

1351 Twomey, S.: The nuclei of natural cloud formation part II: The supersaturation in natural clouds and the
 1352 variation of cloud droplet concentration, Geofis. Pura e Appl., doi:10.1007/BF01993560, 1959.

1353 Twomey, S.: The Influence of Pollution on the Shortwave Albedo of Clouds, J. Atmos. Sci.,
 1354 doi:10.1175/1520-0469(1977)034<1149:TIOPOT>2.0.CO;2, 1977.

1355 Wang, Y., Jiang, J.H., Su, H., Choi, S., Huang, L., Guo, J., and Yung, Y. L.: Elucidating the Role of
 1356 Anthropogenic Aerosols In Arctic Sea Ice Variations, J. Climate 31(1), 99-114, 2018.

1357 Wang, Y., Zheng, X., Dong, X., Xi, B., Wu, P., Logan, T., and Yung, Y. L.: Impacts of long-range
 1358 transport of aerosols on marine-boundary-layer clouds in the eastern North Atlantic, Atmos. Chem.
 1359 Phys., 20, 14741–14755, <https://doi.org/10.5194/acp-20-14741-2020>, 2020.

1360 West, R. E. L., Stier, P., Jones, A., Johnson, C. E., Mann, G. W., Bellouin, N., Partridge, D. G. and
 1361 Kipling, Z.: The importance of vertical velocity variability for estimates of the indirect aerosol
 1362 effects, Atmos. Chem. Phys., doi:10.5194/acp-14-6369-2014, 2014.

1363 Widener, K, Bharadwaj, N, and Johnson, K: Ka-Band ARM Zenith Radar (KAZR) Instrument Handbook.
 1364 DOE ARM Climate Research Facility, DOE/SC-ARM/TR-106, 2012. Available at:
 1365 https://www.arm.gov/publications/tech_reports/handbooks/kazr_handbook.pdf, last access: 23
 1366 April 2021.

1367 Wood, R.: Rate of loss of cloud droplets by coalescence in warm clouds, *J. Geophys. Res. Atmos.*,
1368 doi:10.1029/2006JD007553, 2006.

1369 Wood, R. and Bretherton, C. S.: On the relationship between stratiform low cloud cover and lower-
1370 tropospheric stability, *J. Clim.*, doi:10.1175/JCLI3988.1, 2006.

1371 Wood, R.: Stratocumulus clouds, *Mon. Weather Rev.*, doi:10.1175/MWR-D-11-00121.1, 2012.

1372 Wood, R., Wyant, M., Bretherton, C. S., Rémillard, J., Kollias, P., Fletcher, J., Stemmler, J., De Szoeki,
1373 S., Yuter, S., Miller, M., Mechem, D., Tselioudis, G., Chiu, J. C., Mann, J. A. L., O'Connor, E. J.,
1374 Hogan, R. J., Dong, X., Miller, M., Ghate, V., Jefferson, A., Min, Q., Minnis, P., Palikonda, R.,
1375 Albrecht, B., Luke, E., Hannay, C. and Lin, Y.: Clouds, aerosols, and precipitation in the marine
1376 boundary layer: An arm mobile facility deployment, *Bull. Am. Meteorol. Soc.*, doi:10.1175/BAMS-
1377 D-13-00180.1, 2015.

1378 Wu, P., Dong, X. and Xi, B.: Marine boundary layer drizzle properties and their impact on cloud property
1379 retrieval, *Atmos. Meas. Tech.*, doi:10.5194/amt-8-3555-2015, 2015.

1380 Wu, P., Dong, X., Xi, B., Liu, Y., Thieman, M. and Minnis, P.: Effects of environment forcing on marine
1381 boundary layer cloud-drizzle processes, *J. Geophys. Res.*, doi:10.1002/2016JD026326, 2017.

1382 Wu, P., Dong, X., Xi, B., Tian, J. and Ward, D. M.: Profiles of MBL Cloud and Drizzle Microphysical
1383 Properties Retrieved From Ground-Based Observations and Validated by Aircraft In Situ
1384 Measurements Over the Azores, *J. Geophys. Res. Atmos.*, doi:10.1029/2019JD032205, 2020a.

1385 Wu, P., Dong, X. and Xi, B.: A climatology of marine boundary layer cloud and drizzle properties
1386 derived from ground-based observations over the azores, *J. Clim.*, doi:10.1175/JCLI-D-20-0272.1,
1387 2020b.

1388 Xi, B., Dong, X., Minnis, P. and Khaiyer, M. M.: A 10 year climatology of cloud fraction and vertical
1389 distribution derived from both surface and GOES observations over the DOE ARM SPG site, *J.*
1390 *Geophys. Res. Atmos.*, doi:10.1029/2009JD012800, 2010.

1391 Yang, Y., Zhao, C., Dong, X., Fan, G., Zhou, Y., Wang, Y., Zhao, L., Lv, F. and Yan, F.: Toward
 1392 understanding the process-level impacts of aerosols on microphysical properties of shallow cumulus
 1393 cloud using aircraft observations, *Atmos. Res.*, doi:10.1016/j.atmosres.2019.01.027, 2019.
 1394 Yue, Q., Kahn, B. H., Fetzer, E. J. and Teixeira, J.: Relationship between marine boundary layer clouds
 1395 and lower tropospheric stability observed by AIRS, CloudSat, and CALIOP, *J. Geophys. Res.*
 1396 *Atmos.*, doi:10.1029/2011JD016136, 2011.
 1397 Yum, S. S., Wang, J., Liu, Y., Senum, G., Springston, S., McGraw, R. and Yeom, J. M.: Cloud
 1398 microphysical relationships and their implication on entrainment and mixing mechanism for the
 1399 stratocumulus clouds measured during the VOCALS project, *J. Geophys. Res.*,
 1400 doi:10.1002/2014JD022802, 2015.
 1401 Zhang, S., Wang, M., J. Ghan, S., Ding, A., Wang, H., Zhang, K., Neubauer, D., Lohmann, U., Ferrachat,
 1402 S., Takeamura, T., Gettelman, A., Morrison, H., Lee, Y., T. Shindell, D., G. Partridge, D., Stier, P.,
 1403 Kipling, Z. and Fu, C.: On the characteristics of aerosol indirect effect based on dynamic regimes
 1404 in global climate models, *Atmos. Chem. Phys.*, doi:10.5194/acp-16-2765-2016, 2016.
 1405 Zhao, C., Qiu, Y., Dong, X., Wang, Z., Peng, Y., Li, B., Wu, Z. and Wang, Y.: Negative Aerosol-Cloud
 1406 re Relationship From Aircraft Observations Over Hebei, China, *Earth Sp. Sci.*,
 1407 doi:10.1002/2017EA000346, 2018.
 1408 Zhao, C., Zhao, L. and Dong, X.: A case study of stratus cloud properties using in situ aircraft
 1409 observations over Huanghua, China, *Atmosphere (Basel)*, doi:10.3390/atmos10010019, 2019.
 1410 Zawadowicz, M. A., Suski, K., Liu, J., Pekour, M., Fast, J., Mei, F., Sedlacek, A., Springston, S., Wang,
 1411 Y., Zaveri, R. A., Wood, R., Wang, J., and Shilling, J. E.: Aircraft measurements of aerosol and
 1412 trace gas chemistry in the Eastern North Atlantic, *Atmos. Chem. Phys. Discuss.* [preprint],
 1413 <https://doi.org/10.5194/acp-2020-887>, in review, 2020.
 1414 Zheng, G., Wang, Y., Aiken, A. C., Gallo, F., Jensen, M. P., Kollias, P., Kuang, C., Luke, E., Springston,
 1415 S., Uin, J., Wood, R., and Wang, J.: Marine boundary layer aerosol in the eastern North Atlantic:

seasonal variations and key controlling processes, *Atmos. Chem. Phys.*, 18, 17615–17635,
<https://doi.org/10.5194/acp-18-17615-2018>, 2018.

Zheng, G., Kuang, C., Uin, J., Watson, T., and Wang, J.: Large contribution of organics to condensational
growth and formation of cloud condensation nuclei (CCN) in the remote marine boundary layer,
Atmos. Chem. Phys., 20, 12515–12525, <https://doi.org/10.5194/acp-20-12515-2020>, 2020.

Zheng, X., Xi, B., Dong, X., Logan, T., Wang, Y. and Wu, P.: Investigation of aerosol-cloud interactions
under different absorptive aerosol regimes using Atmospheric Radiation Measurement (ARM)
southern Great Plains (SGP) ground-based measurements, *Atmos. Chem. Phys.*, doi:10.5194/acp-
20-3483-2020, 2020.

Zheng, Y., Rosenfeld, D. and Li, Z.: Quantifying cloud base updraft speeds of marine stratocumulus
from cloud top radiative cooling, *Geophys. Res. Lett.*, doi:10.1002/2016GL071185, 2016.

Zheng, Y., Rosenfeld, D. and Li, Z.: A More General Paradigm for Understanding the Decoupling of
Stratocumulus-Topped Boundary Layers: The Importance of Horizontal Temperature Advection,
Geophys. Res. Lett., doi:10.1029/2020GL087697, 2020.

Zhu, P. and Zuidema, P.: On the use of PDF schemes to parameterize sub-grid clouds, *Geophys. Res.*
Lett., doi:10.1029/2008GL036817, 2009.

Table 1. Dates and time periods of selected non-precipitating MBL cloud periods

Case No.	Start Date	Start UTC	End Date	End UTC	Valid Samples
1	20160915	2200	20160916	0020	24
2	20170219	2110	20170220	0520	87
3	20170222	0830	20170222	1200	38
4	20170605	1430	20170605	1900	54
5	20170616	1230	20170616	1510	32
6	20170617	0320	20170617	0520	24
7	20170627	0020	20170627	0250	28
8	20170630	0530	20170630	0930	42
9	20170630	1400	20170630	1700	34
10	20170706	0140	20170706	0900	62
11	20170707	0130	20170707	1000	91
12	20170910	2100	20170911	0600	94
13	20170911	1930	20170911	2150	24
14	20170912	0820	20170912	1100	32
15	20171006	2110	20171006	2320	26
16	20180130	1030	20180131	0500	152
17	20180203	1930	20180204	0500	72
18	20180324	0210	20180324	0600	46
19	20180508	0730	20180508	1110	42
20	20180513	2130	20180514	1200	139

Table 2. Occurrence frequencies of large in-cloud r_e * under relatively high PWV conditions

PWV (cm)	1.2- 1.4	1.4- 1.6	1.6- 1.8	2.8- 2.0	2.0- 2.2	2.2- 2.4
$r_e > 12 \mu\text{m}$ (%)	25.0	30.6	54.1	74.2	93.8	97.5
$r_e > 14 \mu\text{m}$ (%)	1.25	1.77	7.4	17.7	31.9	20.1

*The occurrence of large r_e is defined when the r_e is found to be larger than $12 \mu\text{m}$ or $14 \mu\text{m}$ using the retrieved in-cloud vertical profiles.

Table 3. ACI_r calculated with respect to N_{CCN} theoretically at different supersaturation levels, under all PWV_{BL} conditions

PWV_{BL} (cm)	0.4-0.6	0.6-0.8	0.8-1.0	1.0-1.2	1.2-1.4	1.4-1.6	1.6-1.8	1.8-2.0	2.0-2.2	2.2-2.4
ACI_r										
$(N_{CCN}@0.2\%SS)$	0.020	0.057	0.002	-0.014	0.108	0.076	0.145	0.151	0.221	0.175
$(N_{CCN}@0.5\%SS)$	0.023	0.057	0.0002	0.024	0.129	0.121	0.309	0.136	0.293	0.159
$(N_{CCN}@1.2\%SS)$	0.023	0.045	0.002	0.072	0.125	0.123	0.323	0.175	0.347	0.186

Table 4. The first three principal components from eigenanalysis

Eigenanalysis	PC1	PC2	PC3
Eigenvalues	2.17	1.10	0.91
Proportion of variance explained (%)	43.72	22.01	18.26
Cumulative proportion (%)	43.72	65.73	83.99
Correlations (Variables vs. PCs)	PC1	PC2	PC3
PWV _{BL}	-0.84	0.20	-0.11
D _i	-0.73	-0.48	-0.20
TKE _W	0.69	0.35	-0.44
W _{dir,ns}	0.52	0.60	-0.50
LTS	-0.43	0.58	0.65

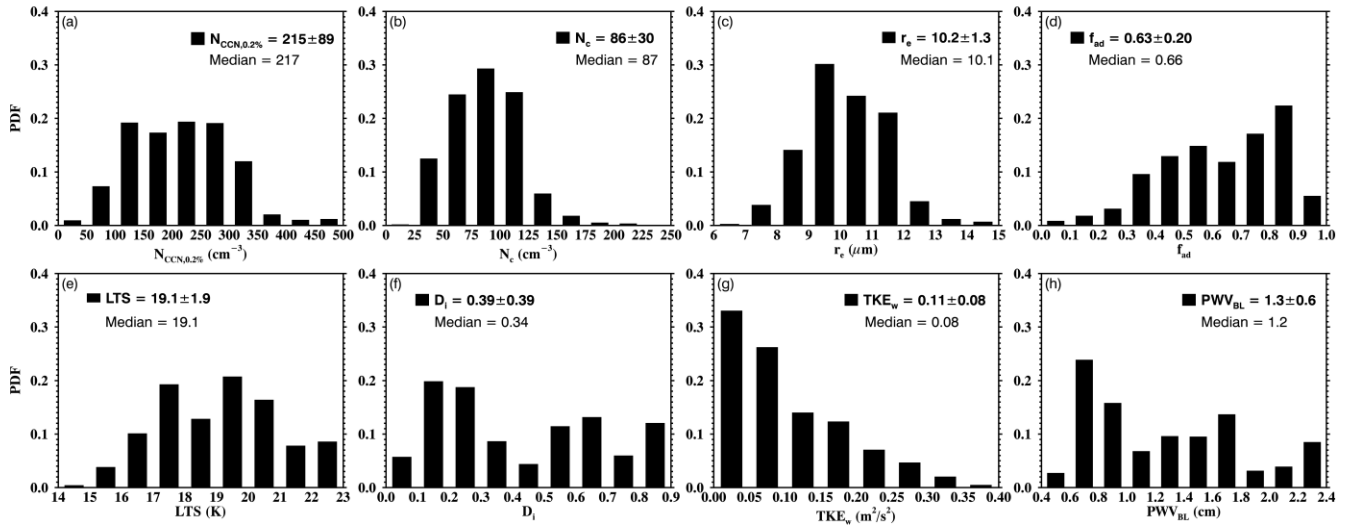


Figure 1. Probability distribution functions (PDFs), mean, standard deviation and median values (dash lines) of aerosol, cloud, and meteorological properties for 20 selected non-precipitating cloud cases at the DOE ENA site during the period 2016-2018. (a) Cloud condensation nuclei (CCN) number concentration at 0.2% supersaturation ($N_{CCN,0.2\%}$); (b) cloud-droplet number concentration (N_c); (c) cloud-droplet effective radius (r_e); (d) cloud adiabaticity (f_{ad}); (e) lower tropospheric stability (LTS); (f) decoupling index (D_i); (g) mean vertical component of turbulence kinetic energy (TKE_w); and (h) sub-cloud boundary-layer precipitable water vapor (PWV_{BL}).

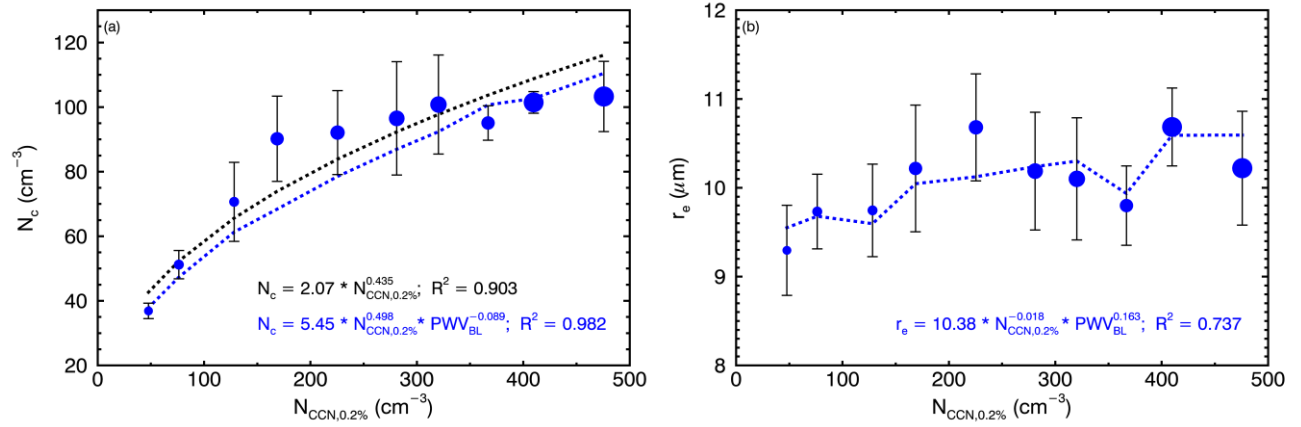


Figure 2. (a) N_c and (b) r_e as a function of $N_{CCN,0.2\%}$ (x-axis) and PWV (blue filled circles) for all selected samples. The larger blue circles represent relatively higher PWV values. Whiskers denote one standard deviation for each bin.

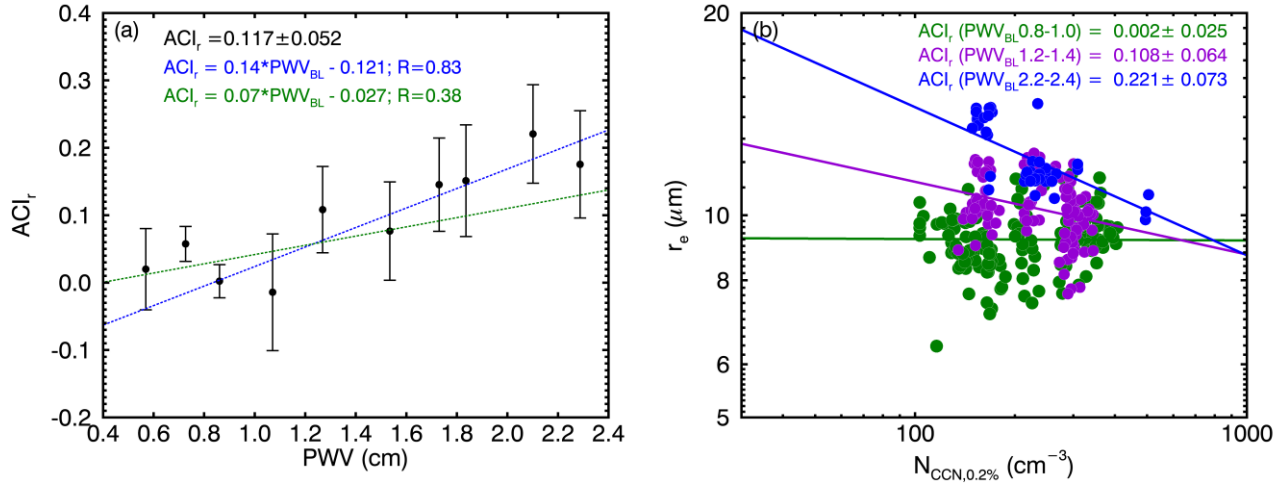


Figure 3. (a) Relationship of ACI_r (dots) to binned PWV_{BL} . Whiskers denote one standard deviation for each bin. Linear regressions are performed in relatively low PWV_{BL} regime (< 1.4 cm, green) and high PWV_{BL} regime (> 1.4 cm); and (b) illustration of ACI_r derived from r_e to $N_{CCN,0.2\%}$ in following three PWV_{BL} bins: 0.8-1.0 cm (green), 1.2-1.4 cm (purple), 2.2-2.4 cm (blue). The ACI_r represents the relative change of r_e with respect to the relative change of $N_{CCN,0.2\%}$, where positive ACI_r denotes the decrease of r_e with increased $N_{CCN,0.2\%}$ under binned PWV.

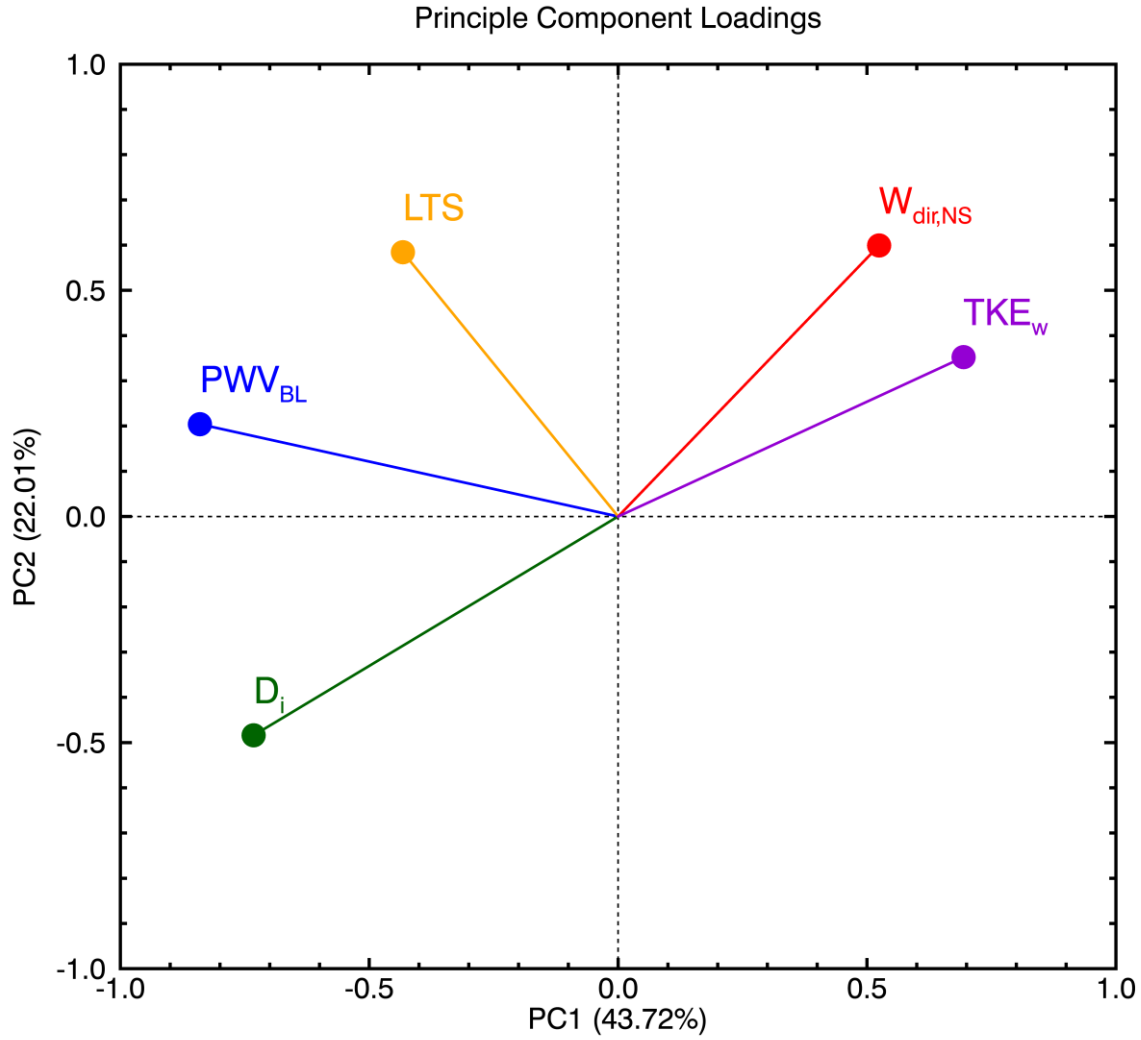


Figure 4. The projections of TKE_w (purple), $W_{dir,NS}$ (red), LTS (orange), PWV_{BL} (blue) and D_i (green) onto the first principal component (PC1) and the second principal component (PC2). The x-coordinates denote variables' correlations with PC1, and the y-coordinates denote variables' correlations with PC2.

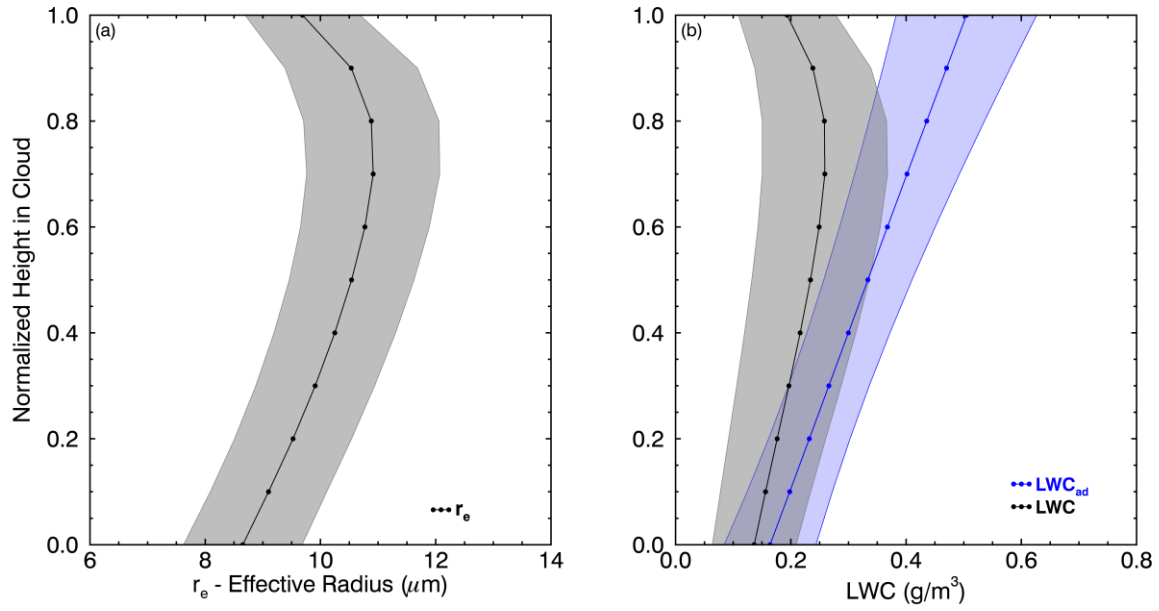


Figure 5. Normalized in-cloud vertical profiles of retrieved (a) r_e and (b) LWC (black) and calculated adiabatic LWC_{ad} (blue) for all selected cloud cases, 0 is cloud base and 1 is cloud top. Solid dotted lines denote mean values and shaded areas denote one standard deviation at each height.

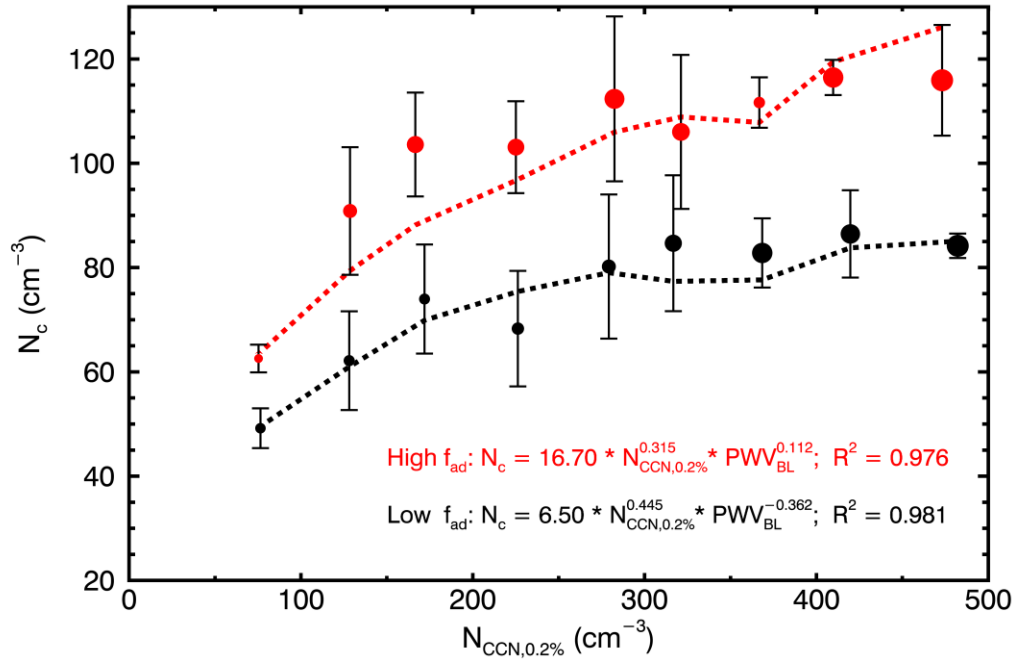


Figure 6. N_c as a function of $N_{CCN,0.2\%}$ (x-axis) and PWV (dots) for high adiabaticity f_{ad} (red) and low f_{ad} (black) regimes. The larger circles represent relatively higher PWV values. Whiskers denote one standard deviation for each bin.

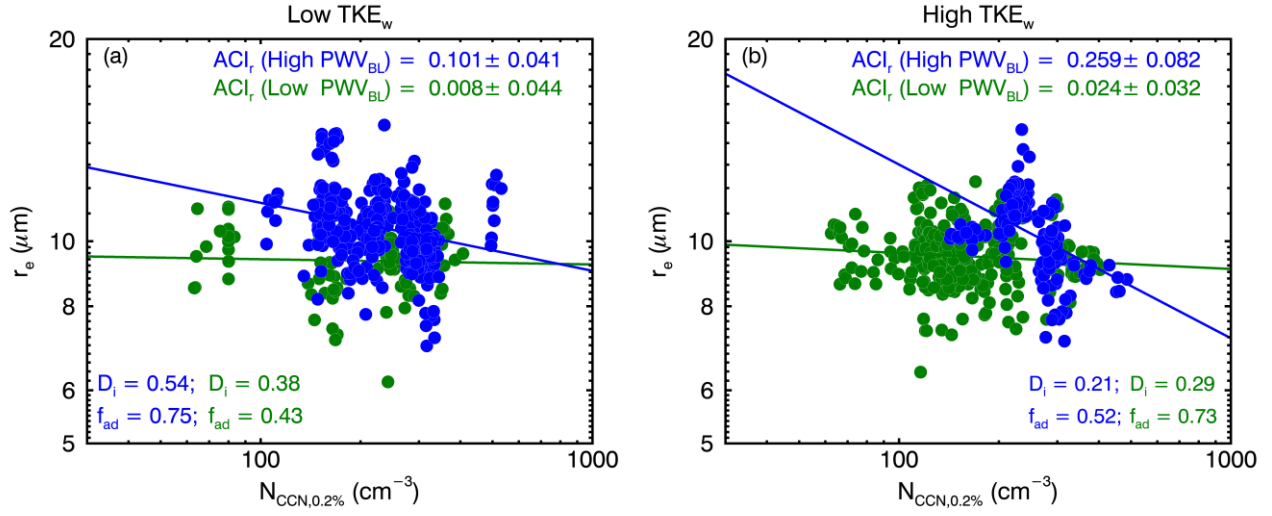


Figure 7. ACI_r derived from r_e to $N_{\text{CCN},0.2\%}$ for (a) low TKE_w and (b) high TKE_w regimes. Samples in the low PWV regime are plotted in green, and samples in the high PWV regime are plotted in blue. The mean values of D_i and f_{ad} are displayed for each quadrant with the corresponding color-coded.

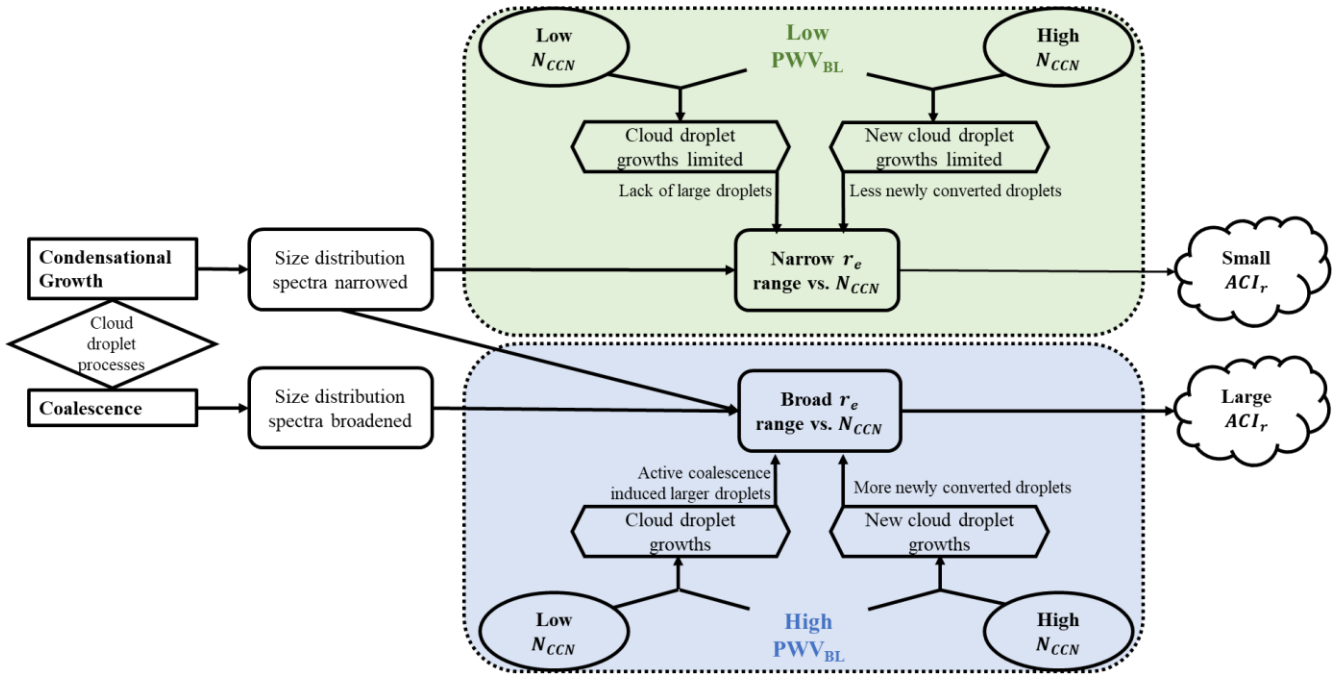


Figure 8. Theoretical mechanism of the responses of cloud droplet size distributions to different CCN intrusion, under relative insufficient (low PWV_{BL}) versus sufficient (high PWV_{BL}) water vapor availabilities.